STATISTICS, OPTIMIZATION AND INFORMATION COMPUTING
Stat., Optim. Inf. Comput., Vol. **16**, August 2026, pp 1350–1378.
Published online in International Academic Press (www.IAPress.org)

Coupled dynamics of dust storms and vegetation: A mathematical approach to restoration

Mohammed Tahseen Hussein [1], Shireen Jawad [1,*], Shubhadeep Ghosh [2], Bapin Mondal[3], Anirban Tarafdar[4]

[1]*Department of Mathematics, College of Science, University of Baghdad, Baghdad, Iraq*
[2]*Department of Mathematics and Statistics, Umeschandra College, Kolkata-12, India*
[3]*Department of Mathematics, School of Computer Science and Artificial Intelligence, SR University, Warangal, Telangana, 506371, India*
[4]*Department of Artificial Intelligence, School of Artificial Intelligence, Amrita Vishwa Vidyapeetham, Faridabad, India*

Abstract Dust storms significantly threaten ecosystems, biodiversity, and human health. Understanding its interactions with plant biomass and revegetation initiatives is crucial for developing effective mitigation strategies. In this study, we present a dynamic Dust Storms-Plant Biomass-Revegetation (SPR) model based on a system of differential equations to explore the relationships among dust storms, vegetation growth, and revegetation activities. The model incorporates key ecological and environmental factors, such as wind effects, logistic growth, Allee thresholds, and saturation dynamics, to reflect real-world complexities. Dust accumulation adversely affects plant health by obstructing photosynthetic processes, whereas vegetation helps reduce dust storms by acting as a natural filter. Revegetation initiatives further enhance the ecosystem's ability to stabilize dust levels and promote plant growth. This study investigates the thresholds and tipping points within the ecosystem that determine its trajectory toward recovery or collapse. Through analytical and numerical methods, we assess the impact of environmental parameters and management strategies on system dynamics. The findings reveal the critical role of vegetation and revegetation in mitigating dust storms and underscore the importance of considering wind, saturation effects, and natural depletion rates in environmental planning. This research provides actionable insights into balancing ecological restoration efforts with dust storm management, contributing to sustainable development goals.

Keywords Stability Analysis, Dust Storms, Wind Speed, Desertification, Dust Pollutants, Revegetation, Plant biomass, Bifurcation Analysis

AMS 2010 subject classifications 34D05, 34D20, 34K18,34K20, 35B35, 34D23

DOI: 10.19139/soic-2310-5070-4164

1. Introduction

Dust storms have become a significant environmental concern, impacting various ecological and human global health. Originating from both natural processes, such as soil erosion and volcanic eruptions, and anthropogenic activities, including industrial operations, mining, and vehicular emissions, dust particles contribute to atmospheric pollution and pose challenges to environmental sustainability [1, 2]. The interactions between dust storms, plant biomass, and revegetation activities are complex and multifaceted, necessitating comprehensive studies to understand their dynamics and inform effective mitigation strategies [3]. The deposition of dust on plant surfaces can adversely affect photosynthesis, transpiration, and overall plant health. Dust particles can obstruct stomatal openings, reducing gas exchange and light absorption, which are critical for photosynthetic processes [4]. Studies have shown that dust accumulation on leaves can lead to a decline in chlorophyll content and photosynthetic

*Correspondence to: Shireen Jawad (Email: shireen.jawad@sc.uobaghdad.edu.iq). Department of Mathematics, College of Science, University of Baghdad, Baghdad, Iraq.

ISSN 2310-5070 (online) ISSN 2311-004X (print)

efficiency, ultimately affecting plant growth and productivity [5]. For instance, research indicates that dust storms can cause a significant reduction in photosynthetic activity in various plant species. For more realistic results, some scholars have discussed the influence of time-varying environments to address periodic or almost periodic oscillations. In addition, the effect of time delay in realistic modeling has been addressed [6, 7, 8, 9].

Conversely, vegetation plays a crucial role in mitigating dust storms. Plants act as natural filters, capturing airborne particles on their surfaces and reducing dust concentrations in the atmosphere. The effectiveness of this natural mitigation depends on factors such as leaf morphology, surface characteristics, and the density of vegetation cover [10]. Research has demonstrated that certain plant species are more efficient in dust interception, contributing to improved air quality. Revegetation initiatives further enhance the capacity of ecosystems to manage dust storms. By increasing plant biomass, revegetation activities not only sequester carbon but also enhance the landscape's ability to capture and stabilize dust particles. This dual benefit underscores the importance of integrating revegetation into environmental management strategies aimed at controlling dust storms and promoting ecological balance [11].

Wind is an important environmental element that has both direct and indirect effects on diverse ecosystems. It helps to carry dust and pollutants, regulates temperature and humidity, and aids in the spread of seeds and germs. To comprehend and forecast these impacts, scientists employ mathematical modeling to describe the link between wind and environmental variables using equations [12], [13]. Wind affects animal behavior, migration, and distribution. Many birds rely on wind direction during migration to conserve energy, while certain insects use wind to get from one location to another. Storms and severe winds, on the other hand, have the potential to damage natural habitats and upset ecological equilibrium. Jawad et al. explored a prey-predator model incorporating the effects of wind, fear, and global warming. They suggest that wind plays a vital role in environmental disturbance and biological processes, including disease, behavior, and growth [14]. Wind aids in the movement of pollen between plants, a process known as wind pollination, which contributes to the reproduction of many plant species, including wheat, maize, and palm trees. Wind also aids the long-distance dispersal of seeds, enhancing plant dispersion and diversity in many habitats. However, high winds can harm plants by breaking branches, uprooting trees, and increasing water loss via transpiration [15].

Mathematical modeling serves as a valuable tool in elucidating the interactions between dust storms, plant biomass, and revegetation activities. By developing dynamic models that incorporate various ecological and environmental parameters, researchers can simulate different scenarios and predict the outcomes of multiple interventions. Such models aid in understanding the potential impacts of dust storms on plant communities and the effectiveness of revegetation strategies in mitigating these effects [16, 17, 18]. Shyam et al. investigated the effect of dust pollution on the density of plant biomass. They considered three variables in their model: the plant biomass, dust contaminants, and water spray. They found that the use of water sprinklers on plants is superfluous when the amount of dust pollutants is below the minimum permissible limit [7].

In this study, we propose a system of differential equations to model the dynamics of dust storms, plant biomass, and revegetation activities with wind and Allee effects' ecological and environmental factors [17, 19]. The model aims to capture the complex interactions among these components, providing insights into the potential outcomes of various environmental management strategies. By analyzing the model's behavior under different scenarios, we seek to inform effective policies and practices for mitigating dust storms and promoting environmental sustainability.

The structure of this paper is as follows: Section 2 presents the mathematical formulation of the model, detailing the assumptions and parameters involved. Section 3-6 discusses the analytical methods used to study the model's behavior, including stability and sensitivity analyses. Section 7 presents the results of numerical simulations, illustrating the potential impacts of different revegetation strategies on dust storms and plant biomass. Finally, Section 8 concludes with a discussion of the findings and their implications for environmental management and policy. By integrating ecological dynamics with mathematical modeling, this research adds to a more profound comprehension of the interplay between dust storms, plant biomass, and revegetation activities. The insights gained from this research can inform the development of effective strategies to mitigate dust storms and promote ecological resilience in affected regions.

2. Model formulation

An SPR model is expressed to describe the interaction among dust storm contamination $S(t)$, plant biomass or vegetation cover $P(t)$, and revegetation activities $R(t)$ at time t based on the ecological assumptions listed below.

1. The rate at which dust contamination is introduced into the atmosphere from diverse sources is represented by A, while μ_0 represents the natural depletion of dust contaminants [2].
2. Vegetation is essential for reducing dust storms. As natural purifiers, plants capture dispersed particles on their surfaces and decrease the amount of dust in the atmosphere. So, the modified Holling II functional response $\left(\frac{\alpha(1+\omega)SP}{1+b(1+\omega)S}\right)$ is used to describe the scavenging of dust pollutants by the vegetation cover. Here α denotes the depletion of dust pollutants owing to plant biomass, and b signifies a half-saturation level [10].
3. The function $G(\omega) = 1 + \omega$ represents the influence of wind flow, which adheres to the following
   - In the absence of wind flow, i.e., $G(0) = 1$, the diminution of dust pollution concentration attributable to plant biomass is $\left(\frac{\alpha SP}{1+bS}\right)$.
   - In the presence of wind flow, i.e., $\acute{G}(\omega) > 1$, the amount of dust particles decreases steadily as a result of plant biomass.
4. It is presumed that the plant population grows logistically with an intrinsic plant growth rate r, carrying capacity k, and the Allee threshold c, and depletion rate μ_1 [17].
5. Dust can hinder photosynthesis in plants. It can block stomatal apertures, decreasing gas exchange and light absorption, which affects photosynthetic processes and plant development. Thus, $\left(\frac{\beta(1+\omega)SP}{1+b(1+\omega)S}\right)$ represents the depletion of plants due to the increase in dust storms, where β denotes the depletion rate of vegetation cover due to a dust storm [7].
   The inclusion of the wind factor $(1+\omega)$ in both the numerator and the denominator were intended to reflect the dual role of wind in the dust-scavenging process by plants. Biologically, moderate wind enhances the transport of dust particles toward the plant surface, thereby increasing the effective contact rate between dust particles and foliage. This effect is represented by the increase in the attack rate through the term $\alpha(1+\omega)$. At the same time, stronger wind conditions may also reduce the efficiency of dust retention due to particle resuspension and shorter residence time of particles near the leaf surface. To capture this saturation-related effect, the same factor was incorporated into the denominator as $b(1+\omega)$, which effectively increases the half-saturation constant. Consequently, the functional response assumes that wind simultaneously promotes dust delivery while also limiting scavenging efficiency at higher dust concentrations. In particular, the chosen formulation allows wind to influence both the encounter process and the saturation dynamics simultaneously, which we consider more biologically realistic for airborne dust–plant interactions.
6. Revegetation initiatives have been implemented to increase plant biomass. Furthermore, it is presumed that specific revegetation initiatives are declining due to inefficiency or financial challenges. The term
$$\frac{dR}{dt} = e(k - P) - \mu_2 R$$
   as intended to represent a management-driven revegetation policy in which restoration efforts increase when plant biomass falls below a desired ecological threshold k. In this interpretation, $e(k-P)$ models a "gap-filling" mechanism: larger vegetation deficits trigger stronger intervention for revegetation. However, as correctly pointed out, this term may become negative when $P > k$, which is biologically unrealistic because implementation effort cannot be negative. So that revegetation occurs only when plant biomass is below the target level k. This modification preserves the intended ecological interpretation while avoiding biologically meaningless negative rates [11].
7. Regarding the plant growth term γPR, we intended to model the enhancement of vegetation recovery through revegetation activities, where R represents the intensity of restoration measures and γ measures their effectiveness in promoting plant establishment. The bilinear form assumes that revegetation effectiveness depends on both the existing plant biomass and the level of restoration activity [10].

8. The implementation rate for revegetation initiatives is presumed to be e, and the decline coefficient for revegetation initiatives is denoted by μ_2 [10].

So, the dynamics of the SPR model could be illustrated as:

$$\begin{aligned}
\frac{dS}{dt} &= A - \frac{\alpha\,(1+\omega)\,SP}{1+b\,(1+\omega)\,S} - \mu_0 S = f_1(S,P),\\
\frac{dP}{dt} &= rP\left(1-\frac{P}{k}\right)\left(\frac{P}{P+c}\right) - \frac{\beta\,(1+\omega)\,SP}{1+b\,(1+\omega)\,S} + \gamma PR - \mu_1 P = f_2(S,P,R),\\
\frac{dR}{dt} &= e\,(k-P) - \mu_2 R = f_3(P,R),
\end{aligned} \tag{1}$$

The explanation of SPR model's parameters is clearly shown in Table 1 below.

Table 1. Overview of the parameters.

Parameters	Meaning	Values	Unit	Source
A	The rate of dust pollutants introduced into the atmosphere from diverse sources.	10	$\mu g m^{-3} day^{-1}$	[7]
α	The depletion rate of dust storms due to plant biomass.	0.25	$m^2 kg^{-1} day^{-1}$	[7]
β	The depletion rate of plant biomass due to a dust storm.	0.4	$m^2 kg^{-1} day^{-1}$	[7]
ω	Wind speed.	3	dimensionless	Estimated from [20]
b	Half saturation level.	0.2	$m^3/\mu g$	[21]
r	Intrinsic growth rate of vegetation.	0.3	day^{-1}	[21]
k	Carrying capacity of plant biomass.	10	kg/m^2	[21]
c	Allee threshold.	0.001	kg/m^2	Estimated from [11]
γ	The revegetation-induced plant biomass growth rate.	0.1	day^{-1}	[10]
e	The implementation rate for revegetation initiatives	0.2	day^{-1}	[10]
μ_0	The natural depletion rate of dust pollutants.	0.03	day^{-1}	[7]
μ_1	The natural depletion rate of plant biomass.	0.02	day^{-1}	[7]
μ_2	The depletion rate of revegetation initiatives.	0.02	day^{-1}	[10]

Furthermore, Figure 1 provides a detailed schematic representation of the SPR system.

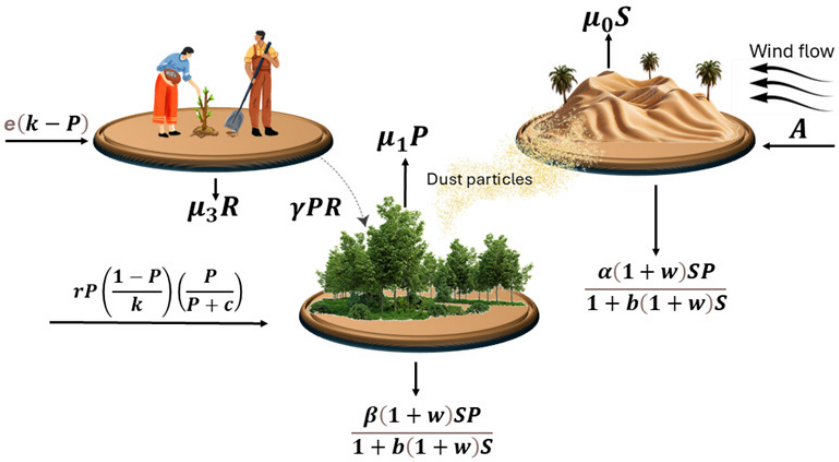

Figure 1. Schematic representation of the SPR system.

3. Model analysis

Theorem 1
The solution $(S(t), P(t), R(t))$ of SPR model with the initial condition $(S_0, P_0, R_0) \in R_+^3$ is positive.

Proof
According to the vegetation cover equation of SPR system, we get

$$P(t) = P_0 \exp\left\{\int_0^t \left(\frac{rP(x)(k-P(x))}{k(P(x)+c)} - \frac{\beta(1+\omega)S(x)}{1+b(1+\omega)S(x)} + \gamma R(x) - \mu_1\right)dx\right\} > 0.$$

From the dust storm equation, we attain

$$dS = \left(A - \frac{\alpha(1+\omega)SP}{1+b(1+\omega)S} - \mu_0 S\right)dt \Longrightarrow dS = \left[A - S\left(\mu_0 - \frac{\alpha(1+\omega)}{1+b(1+\omega)S}P\right)\right]dt$$

That means

$$dS \geq -S\left(\mu_0 - \frac{\alpha(1+\omega)}{1+b(1+\omega)S}P\right)dt$$

Subsequently, the formula of $P(t)$ is substituted into $S(t)$ to integrate the equation above, yielding

$$S(t) \geq S_0 \exp\left\{\int_0^t -\left(\mu_0 - \frac{\alpha(1+\omega)}{1+b(1+\omega)S(x)}\left(P_0\, e^{\int_0^t \left(\frac{rP(x)(k-P(x))}{k(P(x)+c)} - \frac{\beta(1+\omega)S(x)}{1+b(1+\omega)S(x)} + \gamma R(x) - \mu_1\right)dx}\right)\right)dx\right\} > 0$$

Finally, from the revegetation equation, we attain

$$R(t) \geq R_0 \exp\left\{\int_0^t -\mu_2 dx\right\} > 0.$$

Thus, the solution $(S(t),\ P(t), R(t))$ will remain positive for all $t \geq 0$. □

Theorem 2
All solutions $(S(t), P(t), R(t))$ of SPR model are uniformly bounded.

Proof
From the dust storm and revegetation equations of the SPR model, we obtain

$$\frac{dS}{dt} = A - \frac{\alpha(1+\omega)SP}{1+b(1+\omega)S} - \mu_0 S \leq\ A - \mu_0 S \Longrightarrow \lim_{t\to\infty} \sup S(t) \leq \frac{A}{\mu_0},$$

and

$$\lim_{t\to\infty} \sup R(t) \leq \frac{ek}{\mu_2}.$$

From the vegetation cover equation, we get

$$\frac{dP}{dt} = rP\left(1 - \frac{P}{k}\right)\left(\frac{P}{P+c}\right) - \frac{\beta(1+\omega)SP}{1+b(1+\omega)S} + \gamma PR - \mu_1 P \leq rP\left(1 - \frac{P}{k}\right)\left(\frac{P}{P+c}\right)$$

$$\Longrightarrow \frac{dP}{dt} \leq rP\left(1 - \frac{P}{k}\right) \Longrightarrow \lim_{t\to\infty} \sup\left[P(t)\right] \leq k.$$

Hence, the attracting region for the SPR system is

$$\varphi = \left\{(S,\ P, R) \in R_+^3 :\ S(t) \leq \frac{A}{\mu_0},\ P(t) \leq k, R(t) \leq \frac{ek}{\mu_2}\right\}.$$

□

4. Equilibria analysis

The possible equilibria of SPR system are

1. The desertification point $H_1 = (S_1, 0, 0)$, where $S_1 = \frac{A}{\mu_0}$.
2. The plant-free point $H_2 = (S_2, 0, R_2)$ where $S_2 = \frac{A}{\mu_0}, R_2 = \frac{ek}{\mu_2}$.
3. The revegetation-free point $H_3 = (S_3, P_3, 0)$, where S_3 and P_3 are the solutions of the following equations

$$A - \frac{\alpha(1+\omega)SP}{1+b(1+\omega)S} - \mu_0 S = 0 \tag{a}$$

$$rP\left(1-\frac{P}{k}\right)\left(\frac{P}{P+c}\right) - \frac{\beta(1+\omega)SP}{1+b(1+\omega)S} - \mu_1 P = 0, \tag{b}$$

From (a), we get

$$P_3 = \frac{A - S\left[\mu_0 - Ab(1+\omega) + \mu_0 b(1+\omega)S\right]}{\alpha(1+\omega)S}, \tag{c}$$

Substituting (c) in (b), we get the following equation:

$$Y_1(S) = c_1S^5 + c_2S^4 + c_3S^3 + c_4S^2 + c_5S + c_6\ ,$$

where

$$\begin{aligned}
c_1 &= -r\mu_0^2b^3(1+\omega)^3\\
c_2 &= \mu_0 b(1+\omega)^2\left[(1+\omega)\left[2Arb^2 - rk\alpha b + \mu_1 k\alpha b + \alpha\beta k\right] - 3r\mu_0 b\right]\\
c_3 &= (1+\omega)\Big[(1+\omega)\left[6Ar\mu_0b^2 - 2\mu_0 rk\alpha b + 2\mu_0\mu_1 k\alpha b + \mu_0\alpha\beta k\right]\\
&\qquad + (1+\omega)^2\left[-rA^2b^3 - A\mu_1 k\alpha b^2 - A\alpha\beta kb - \mu_1 ck\alpha^2 b - \alpha^2\beta ck\right]\Big] + Ark\alpha b^2 - 3r\mu_0 b^2\\
c_4 &= (1+\omega)\left[(1+\omega)\left[2Ar\alpha kb - 3rA^2b^2 - 2A\mu_1\alpha kb - A\alpha\beta k - \mu_1 ck\alpha^2\right] + 6Ar\mu_0 b - \mu_0 r\alpha k + \mu_0\mu_1\alpha k\right] - r\mu^2\\
c_5 &= A(1+\omega)\left[r\alpha k - 3Arb - \mu_1\alpha k\right] + 2Ar\mu_0\\
c_6 &= -A^2r
\end{aligned}$$

Clearly, $Y_1(0) = -A^2r < 0$, and

$$\begin{aligned}
Y_1(A) &= -r\mu_0^2b^3(1+\omega)^3A^5 + \mu_0 b(1+\omega)^2\left[(1+\omega)\left[2Arb^2 - rk\alpha b + \mu_1 k\alpha b + \alpha\beta k\right] - 3r\mu_0 b\right]\\
&A^4 + (1+\omega)\Big[(1+\omega)\left[6Ar\mu_0b^2 - 2\mu_0 rk\alpha b + 2\mu_0\mu_1 k\alpha b + \mu_0\alpha\beta k\right]\\
&\qquad + (1+\omega)^2\left[-rA^2b^3 - A\mu_1 k\alpha b^2 - A\alpha\beta + Ark\alpha b^2 - 3r\mu_0 b^2A^3kb - \mu_1 ck\alpha^2 b - \alpha^2\beta ck\right]\Big]\\
&\qquad + \Big((1+\omega)\left[(1+\omega)\left[2Ar\alpha kb - 3rA^2b^2 - 2A\mu_1\alpha kb - A\alpha\beta k - \mu_1 ck\alpha^2\right]\right.\\
&\qquad \left. + 6Ar\mu_0 b - \mu_0 r\alpha k + \mu_0\mu_1\alpha k\right] - r\mu^2\Big)A^2\\
&\qquad + \left(A(1+\omega)\left[r\alpha k - 3Arb - \mu_1\alpha k\right] + 2Ar\mu_0\right)A - A^2r.
\end{aligned}$$

and

$$Y_1'(S) = 5c_1S^4 + 4c_2S^3 + 3c_3S^2 + 2c_4S + c_5$$

Therefore, by the intermediate value theorem [22], $Y_1(S)$ has a positive root, say S_3 in the interval $(0, A)$ if the following conditions are satisfied:

$$Y_1(A) > 0 \text{ and } Y_1'(S) > 0. \tag{2}$$

For P_3 to be positive, the following must be satisfied:

$$A > S_3 \left[\mu_0 - Ab\left(1+\omega\right) + \mu_0 b\left(1+\omega\right) S_3\right] \tag{3}$$

4. The coexistence point $H_4 = (S_4, P_4, R_4)$, where S_4, P_4 and R_4 are the solutions of the following equations

$$A - \frac{\alpha\left(1+\omega\right)SP}{1+b\left(1+\omega\right)S} - \mu_0 S = 0, \tag{d}$$

$$r\left(1-\frac{P}{k}\right)\left(\frac{P}{P+c}\right) - \frac{\beta\left(1+\omega\right)S}{1+b\left(1+\omega\right)S} + \gamma R - \mu_1 = 0 \tag{e}$$

$$e\left(k-P\right) - \mu_2 R = 0. \tag{f}$$

From (f), we get $R_4 = \frac{e(k-P_4)}{\mu_2}$ and from (d), we get

$$e\left(k-P\right) - \mu_2 R = 0. \tag{g}$$

+ Substituting (g) and (f) in equation (e), we get the following equation:

$$Y_2\left(S\right) = d_1 S^5 + d_2 S^4 + d_3 S^3 + d_4 S^2 + d_5 S + d_6\ ,$$

where

$$\begin{aligned}
d_1 &= -\mu_0^2 b^3\left(1+\omega\right)^3\left[r\mu_2 + \gamma ek\right]\\
d_2 &= \mu_0 b\left(1+\omega\right)^2\Big[-3r\mu_0\mu_2 b - 3\gamma ek\mu_0 b + \left(1+\omega\right)\left[2Ar\mu_2 b^2 + 2A\gamma ekb^2 - rk\mu_2\alpha b - \gamma ek^2\alpha b\right.\\
&\qquad\left. + \gamma ekc\alpha b + \mu_1\mu_2\alpha kb + \alpha\beta k\mu_2\right]\Big]\\
d_3 &= \left(1+\omega\right)\Big[-3r\mu_0^2\mu_2 b - 3\gamma ek\mu_0^2 b + \mu_0\left(1+\omega\right)\left[6Ar\mu_2 b^2 + 6A\gamma ekb^2 - 2rk\mu_2\alpha b - 2\gamma ek^2\alpha b\right.\\
&\qquad\left. + 2\gamma ekc\alpha b + 2\mu_1\mu_2 k\alpha b + \alpha\beta k\mu_2\right] + \left(1+\omega\right)^2\left[Ark\mu_2\alpha b^2 - A^2 r\mu_2 b^3 + A\gamma ek^2\alpha b^2\right.\\
&\qquad\left. - A^2\gamma ekb^3 - A\gamma ekc\alpha b^2 - A\mu_1\mu_2\alpha kb^2 - A\alpha\beta k\mu_2 b - \alpha^2\beta ck\mu_2 + \alpha^2\gamma ek^2 cb - \alpha^2\mu_1\mu_2 kcb\right]\Big]\\
d_4 &= \left(1+\omega\right)\Big[6Ar\mu_0\mu_2 b + 6A\gamma ek\mu_0 b - rk\mu_0\mu_2\alpha - \gamma ek^2\alpha\mu_0 + \gamma ekc\alpha\mu_0 + \mu_0\mu_1\mu_2 k\alpha + \left(1+\omega\right)\left[2Ark\mu_2\alpha b\right.\\
&\qquad\left. + 2A\gamma ek^2\alpha b - 3A^2 r\mu_2 b^2 - 3A^2\gamma ekb^2 - 2A\gamma ekc\alpha b - 2A\mu_1\mu_2 k\alpha b - A\alpha\beta k\mu_2\right.\\
&\qquad\left. + \alpha^2\gamma ek^2 c - \alpha^2\mu_1\mu_2 kc\right]\Big] - \mu_0^2\left[r\mu_2 + \gamma ek\right]\\
d_5 &= A\left(1+\omega\right)\left[-3Ar\mu_2 b - 3A\gamma ekb + r\mu_2\alpha + \gamma ek^2\alpha - \gamma ekc\alpha - \mu_1\mu_2 k\alpha\right]\\
&\quad + 2A\mu_0\left[r\mu_2 + \gamma ek\right] d_6 = -A^2\left[r\mu_2 + \gamma ek\right]
\end{aligned}$$

Clearly,

$$Y_2\left(0\right) = -A^2\left[r\mu_2 + \gamma ek\right] < 0$$

$$
\begin{aligned}
Y_2(A) = &-\mu_0^2 b^3 (1+\omega)^3 [r\mu_2 + \gamma ek] A^5 \\
&+ \mu_0 b (1+\omega)^2 \Big[-3r\mu_0\mu_2 b - 3\gamma ek\mu_0 b + (1+\omega) \big[2Ar\mu_2 b^2 + 2A\gamma ekb^2 - rk\mu_2\alpha b - \gamma ek^2\alpha b \\
&\qquad + \gamma ekc\alpha b + \mu_1\mu_2\alpha kb + \alpha\beta k\mu_2\big]\Big] A^4 \\
&+ (1+\omega) \Big[-3r\mu_0^2\mu_2 b - 3\gamma ek\mu_0^2 b + \mu_0 (1+\omega) \big[6Ar\mu_2 b^2 + 6A\gamma ekb^2 - 2rk\mu_2\alpha b \\
&- 2\gamma ek^2\alpha b + 2\gamma ekc\alpha b + 2\mu_1\mu_2 k\alpha b + \alpha\beta k\mu_2\big] + (1+\omega)^2 \big[Ark\mu_2\alpha b^2 - A^2 r\mu_2 b^3 \\
&+ A\gamma ek^2\alpha b^2 - A^2\gamma ekb^3 - A\gamma ekc\alpha b^2 - A\mu_1\mu_2\alpha kb^2 \\
&- A\alpha\beta k\mu_2 b - \alpha^2\beta ck\mu_2 + \alpha^2\gamma ek^2 cb - \alpha^2\mu_1\mu_2 kcb\big]\Big] A^3 \\
&+ \Big((1+\omega) \Big[6Ar\mu_0\mu_2 b + 6A\gamma ek\mu_0 b - rk\mu_0\mu_2\alpha - \gamma ek^2\alpha\mu_0 + \gamma ekc\alpha\mu_0 + \mu_0\mu_1\mu_2 k\alpha + (1+\omega) \big[2Ark\mu_2\alpha b \\
&+ 2A\gamma ek^2\alpha b - 3A^2 r\mu_2 b^2 - 3A^2\gamma ekb^2 - 2A\gamma ekc\alpha b - 2A\mu_1\mu_2 k\alpha b - A\alpha\beta k\mu_2 + \alpha^2\gamma ek^2 c - \alpha^2\mu_1\mu_2 kc\big]\Big] \\
&- \mu_0^2 [r\mu_2 + \gamma ek]\Big) A^2 + \Big(A(1+\omega) \big[-3Ar\mu_2 b - 3A\gamma ekb + r\mu_2\alpha + \gamma ek^2\alpha - \gamma ekc\alpha - \mu_1\mu_2 k\alpha\big] \\
&+ 2A\mu_0 [r\mu_2 + \gamma ek]\Big) A - A^2 [r\mu_2 + \gamma ek].
\end{aligned}
$$

$$
Y_2'(S) = 5d_1 S^4 + 4d_2 S^3 + 3d_3 S^2 + 2d_4 S + d_5.
$$

Therefore, by the intermediate value theorem, $Y_2(S)$ has a positive root, say S_4 in the interval $(0, A)$ if the following conditions are satisfied:

$$
Y_2(A) > 0 \text{ and } Y_2'(S) > 0. \tag{4}
$$

For P_4 to be positive, the following must be satisfied:

$$
A > S_4 [\mu_0 - Ab(1+\omega) + \mu_0 b(1+\omega) S_4]. \tag{5}
$$

In Figure 2, we present the nullclines of our proposed system, where we observe the existence of one top-predator–free planar equilibrium and one interior equilibrium point.

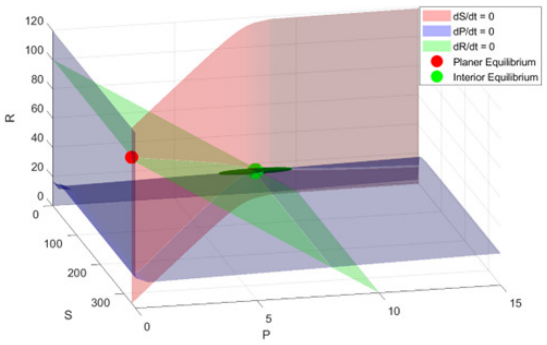

Figure 2. Equilibrium point(s) of the SPR system.

5. Local stability

The Jacobian matrix at any point is used to investigate the local stability of equilibria. Thus, the Jacobian matrix at (S,P,R) is given by

$$J=\begin{bmatrix} -\mu_0-\frac{\alpha(1+\omega)P}{[1+S(b+b\omega)]^2} & \frac{-\alpha(1+\omega)S}{1+S(b+b\omega)} & 0 \\ -\frac{\beta(1+\omega)P}{[1+bS(1+\omega)]^2} & \frac{rP[k(P+2c)-P(2P+3c)]}{k(P+c)^2}-\frac{\beta(1+\omega)S}{1+b(1+\omega)S}+\gamma R-\mu_1 & \gamma P \\ 0 & -e & -\mu_2 \end{bmatrix}. \tag{6}$$

- The Jacobian matrix at $H_1=(S_1,0,0)$ is given as:

$$J(H_1)=\begin{bmatrix} -\mu_0 & -\frac{\alpha A(1+\omega)}{\mu_0+bA(1+\omega)} & 0 \\ 0 & -\frac{\beta A(1+\omega)}{\mu_0+bA(1+\omega)}-\mu_1 & 0 \\ 0 & -e & -\mu_2 \end{bmatrix} \tag{7}$$

Then, the eigenvalues of $J(H_1)$ are $\lambda_1^1=-\mu_0<0, \lambda_2^1=-\frac{\beta A(1+\omega)}{\mu_0+bA(1+\omega)}-\mu_1 and \lambda_3^1=-\mu_2<0$. Therefore, S_1 is asymptotically stable

- The Jacobian matrix at $H_2=(S_2,0,R_2)$ is given as:

$$J(H_2)=\begin{bmatrix} -\mu_0 & -\frac{\alpha\ A(1+\omega)}{\mu_0+bA(1+\omega)} & 0 \\ 0 & -\frac{\beta\ A(1+\omega)}{\mu_0+bA(1+\omega)}+\frac{\gamma\ ek}{\mu_2}-\mu_1 & 0 \\ 0 & -e & -\mu_2 \end{bmatrix} \tag{8}$$

$\lambda_1^2=-\mu_0<0, \lambda_2^2=-\frac{\beta A(1+\omega)}{\mu_0+bA(1+\omega)}+\frac{\gamma ek}{\mu_2}-\mu_1$ and $\lambda_3^2=-\mu_2<0$. Therefore, S_2 is asymptotic stable if

$$\frac{\gamma ek}{\mu_2}<\frac{\beta A(1+\omega)}{\mu_0+bA(1+\omega)}+\mu_1. \tag{9}$$

- The Jacobian matrix at $H_3=(S_3,P_3,0)$ is defined as:

$$J(H_3)=\begin{bmatrix} -\mu_0-\frac{\alpha P_3(1+\omega)}{[1+bS_3(1+\omega)]^2} & \frac{-\alpha S_3(1+\omega)}{1+bS_3(1+\omega)} & 0 \\ -\frac{\beta P_3(1+\omega)}{[1+bS_3(1+\omega)]^2} & \frac{rckP_3-2rcP_3^2-rP_3^3}{k(P_3+c)^2} & \gamma P_3 \\ 0 & -e & -\mu_2 \end{bmatrix}, \tag{10}$$

So, the roots of the following equation are the eigenvalues of $J(H_3)$

$$\lambda^3+F_1\lambda^2+F_2\lambda+F_3=0, \tag{11}$$

where

$$\begin{aligned} F_1&=\mu_0+\frac{\alpha P_3(1+\omega)}{[1+bS_3(1+\omega)]^2}-\frac{rP_3\left(ck-2cP_3-P_3^2\right)}{k(P_3+c)^2}+\mu_2,\\ F_2&=\left(-\mu_0-\frac{\alpha P_3(1+\omega)}{[1+bS_3(1+\omega)]^2}\right)\left(\frac{rP_3\left(ck-2cP_3-P_3^2\right)}{k(P_3+c)^2}\right)\\ &\quad+\left(\mu_0\mu_2+\frac{\alpha P_3(1+\omega)\mu_2}{[1+bS_3(1+\omega)]^2}\right)-\left(\frac{rP_3\left(ck-2cP_3-P_3^2\right)\mu_2}{k(P_3+c)^2}\right)+\gamma eP_3-\frac{\alpha\beta P_3S_3(1+\omega)^2}{[1+bS_3(1+\omega)]^3},\\ F_3&=\left(-\mu_0-\frac{\alpha P_3(1+\omega)}{[1+bS_3(1+\omega)]^2}\right)\left(\frac{rP_3\left(ck-2cP_3-P_3^2\right)\mu_2}{k(P_3+c)^2}-\gamma eP_3\right)-\frac{\alpha\beta P_3S_3(1+\omega)^2\mu_2}{[1+bS_3(1+\omega)]^3}, \end{aligned}$$

$$
\begin{aligned}
F_1F_2 - F_3 =& 2\left(-\mu_0 - \frac{\alpha P_3\left(1+\omega\right)}{\left[1+bS_3\left(1+\omega\right)\right]^2}\right)\left(\frac{rP_3\left(ck-2cP_3-P_3^2\right)\mu_2}{k\left(P_3+c\right)^2}\right)\\
&-\left(\left(-\mu_0 - \frac{\alpha P_3\left(1+\omega\right)}{\left[1+bS_3\left(1+\omega\right)\right]^2}\right)^2 + \gamma e P_3\right)\left(\frac{rP_3\left(ck-2cP_3-P_3^2\right)}{k\left(P_3+c\right)^2} - \mu_2\right)\\
&+\left(\frac{\alpha\beta P_3S_3\left(1+\omega\right)^2}{\left[1+bS_3\left(1+\omega\right)\right]^3} - {\mu^2}_2\right)\left(-\mu_0 - \frac{\alpha P_3\left(1+\omega\right)}{\left[1+bS_3\left(1+\omega\right)\right]^2} + \frac{rP_3\left(ck-2cP_3-P_3^2\right)}{k\left(P_3+c\right)^2}\right)\\
&-\left(\frac{rP_3\left(ck-2cP_3-P_3^2\right)}{k\left(P_3+c\right)^2}\right)^2 - \left(-\mu_0 - \frac{\alpha P_3\left(1+\omega\right)}{\left[1+bS_3\left(1+\omega\right)\right]^2} - \mu_2\right).
\end{aligned}
$$

Thus, using the Routh-Hurwitz rule [23], H_3 will be asymptotically stable if $F_1 > 0, F_3 > 0$ and $F_1F_2 > F_3$.

- The Jacobian matrix at $H_4 = (S_4, P_4, R_4)$ is given as:

$$
J\left(H_4\right) = \begin{bmatrix} -\mu_0 - \frac{\alpha P_4(1+\omega)}{[1+bS_4(1+\omega)]^2} & \frac{-\alpha S_4(1+\omega)}{1+bS_4(1+\omega)} & 0 \\ -\frac{\beta P_4(1+\omega)}{[1+bS_4(1+\omega)]^2} & \frac{rckP_4-2rcP_4^2-rP_4^3}{k(P_4+c)^2} & \gamma P_4 \\ 0 & -e & -\mu_2 \end{bmatrix} \tag{12}
$$

So, the roots of the following equation are the eigenvalues of $J\left(H_4\right)$

$$
\lambda^3 + Z_1\lambda^2 + Z_2\lambda + Z_3 = 0, \tag{13}
$$

where,

$$
\begin{aligned}
Z_1 &= \mu_0 + \mu_2 + \frac{\alpha P_4\left(1+\omega\right)}{\left[1+bS_4\left(1+\omega\right)\right]^2} - \frac{rP_4(ck-2cP_4-P_4^2)}{k\left(P_4+c\right)^2},\\
Z_2 &= \left(\frac{-\alpha P_4\left(1+\omega\right)}{\left[1+bS_4\left(1+\omega\right)\right]^2} - \mu_0\right)\left(\frac{rP_4\left(ck-2cP_4-P_4^2\right)}{k\left(P_4+c\right)^2}\right)\\
&\quad + \left(\mu_0\mu_2 + \frac{\alpha P_4\left(1+\omega\right)\mu_2}{\left[1+bS_4\left(1+\omega\right)\right]^2}\right) - \left(\frac{rP_4\left(ck-2cP_4-P_4^2\right)\mu_2}{k\left(P_4+c\right)^2}\right) + \gamma e P_4 - \frac{\alpha\beta P_4S_4\left(1+\omega\right)^2}{\left[1+bS_4\left(1+\omega\right)\right]^3},\\
Z_3 &= \mu_2\left(\frac{rP_4\left(ck+2cP_4+P_4^2\right)}{k\left(P_4+c\right)^2}\right)\left(\frac{\alpha P_4\left(1+\omega\right)}{\left[1+bS_4\left(1+\omega\right)\right]^2}+\mu_0\right) + e\gamma P_4\left(\frac{\alpha P_4\left(1+\omega\right)}{\left[1+bS_4\left(1+\omega\right)\right]^2} + \mu_0\right)\\
&\quad - \frac{\alpha\beta P_4S_4\left(1+\omega\right)^2\mu_2}{\left[1+bS_4\left(1+\omega\right)\right]^3}.
\end{aligned}
$$

$$
\begin{aligned}
Z_1Z_2 - Z_3 =& 2\mu_2\left(\frac{rP_4\left(ck-2cP_4-P_4^2\right)}{k\left(P_4+c\right)^2}\right)\left(\frac{-\alpha P_4\left(1+\omega\right)}{\left[1+bS_4\left(1+\omega\right)\right]^2} - \mu_0\right)\\
&-\left(\left(\frac{\alpha P_4\left(1+\omega\right)}{\left[1+bS_4\left(1+\omega\right)\right]^2} + \mu_0\right)^2 + \gamma e P_4\right)\left(\frac{rP_4\left(ck-2cP_4-P_4^2\right)}{k\left(P_4+c\right)^2} - \mu_2\right)\\
&+\left(\frac{\alpha\beta S_4P_4\left(1+\omega\right)^2}{\left[1+bS_4\left(1+\omega\right)\right]^3} - {\mu^2}_2\right)\left(\left(\frac{-\alpha P_4\left(1+\omega\right)}{\left[1+bS_4\left(1+\omega\right)\right]^2} - \mu_0\right) + \left(\frac{rP_4\left(ck-2cP_4-P_4^2\right)}{k\left(P_4+c\right)^2}\right)\right)\\
&+\left(\mu_0+\mu_2+\frac{\alpha P_4\left(1+\omega\right)}{\left[1+bS_4\left(1+\omega\right)\right]^2}\right)\left(\frac{rP_4\left(ck-2cP_4-P_4^2\right)}{k\left(P_4+c\right)^2}\right)^2.
\end{aligned}
$$

Thus, H_4 is locally asymptotically stable if $Z_1 > 0, Z_3 > 0$, and $Z_1Z_2 > Z_3$.

6. Basin of attraction

In dynamical systems, a basin of attraction is the set of all initial conditions that eventually evolve toward the same long-term behavior. The basin of attraction of equilibria is analyzed by the Lyapunov approach, as shown in the subsequent theorems [24].

Theorem 3
The basin of attraction of the desertification point $H_1 = (S_1,\ 0, 0)$ is the sub-region of $\vartheta_1 \subset R_+^3$ which satisfies the following condition:

$$\left.\begin{array}{c} \left(\frac{\alpha S(1+\omega)}{1+b(1+\omega)S}\right)^2 \leq \frac{r\mu_0}{(P+c)} \\ \frac{rkP}{(P+c)} + ek + \gamma PR < \mu_1 P \end{array}\right\}. \tag{14}$$

Then, the desertification point $H_1 = (S_1, 0, 0)$ is a GAS (a global asymptotic stability).

Proof
Define $B_1(t) = \frac{(S-S_1)^2}{2} + P + R$, where $B_1(t)$ is a positive definite function about H_1. Thus,

$$\begin{aligned} \frac{dB_1}{dt} =& (S - S_1)\frac{dS}{dt} + \frac{dP}{dt} + \frac{dR}{dt} \Rightarrow \frac{dB_1}{dt} \\ =& (S - S_1)\left[A - \frac{\alpha(1+\omega)SP}{1+b(1+\omega)S} - \mu_0 S - A + \mu_0 S_1\right] \\ &+ P\left[r\left(\frac{k-P}{k}\right)\left(\frac{P}{P+c}\right) - \frac{\beta(1+\omega)S}{1+b(1+\omega)S} + \gamma R - \mu_1\right] + [e(k-P) - \mu_2 R] \end{aligned}$$

i.e.,

$$\begin{aligned} \frac{dB_1}{dt} =& -\left(\mu_0(S-S_1)^2 + \left[\frac{\alpha S(1+\omega)}{1+b(1+\omega)S}\right]P(S-S_1) + \frac{rP^2}{(P+c)}\right) \\ &- \frac{\beta SP(1+\omega)}{1+b(1+\omega)S} + \left(\frac{rkP}{(P+c)} + ek + \gamma PR - \mu_1 P\right) - eP - \mu_2 R \end{aligned}$$

Then, $^{dB_1}/_{dt}$ under condition (14), Therefore, any solution starting from ϑ_1 approach asymptotically to H_1. □

Theorem 4
The basin of attraction of the plant-free point $H_2 = (S_2, 0, R_2)$ is the sub-region of $\vartheta_2 \subset R_+^3$ which satisfies the following condition:

$$\max\left\{\frac{2e^2}{\mu_2}, \left(\frac{2}{\mu_0}\right)\left[\frac{\alpha S(1+\omega)}{1+b(1+\omega)S}\right]^2\right\} \leq \frac{r}{(P+c)} \leq \frac{\mu_1 - \gamma R}{k} \tag{15}$$

Proof
Define $B_2 = \frac{(S-S_2)^2}{2} + P + \frac{(R-R_2)^2}{2}$, where B_2 is a positive definite function about H_2. Thus,

$$\frac{dB_2}{dt} = (S - S_2)\frac{dS}{dt} + \frac{dP}{dt} + (R - R_2)\frac{dR}{dt}$$

i.e.,

$$\begin{aligned} \frac{dB_2}{dt} =& (S - S_2)\left[A - \mu_0 S - \frac{\alpha(1+\omega)SP}{1+b(1+\omega)S} - A + \mu_0 S_2\right] \\ &+ \left[rP\left(\frac{k-P}{k}\right)\left(\frac{P}{P+c}\right) - \frac{\beta(1+\omega)SP}{1+b(1+\omega)S} + \gamma PR - \mu_1 P\right] \\ &+ (R - R_2)[ek - eP - \mu_2 R - ek + \mu_2 R_2]. \end{aligned}$$

Therefore,

$$\begin{aligned}\frac{dB_2}{dt} \leq & -\left(\mu_0 (S-S_2)^2 + \left[\frac{\alpha S(1+\omega)}{1+b(1+\omega)S}\right](S-S_2)P + \frac{r}{2(P+c)}P^2\right) \\ & -\left(\mu_2 (R-R_2)^2 + eP(R-R_2) + \frac{r}{2(P+c)}P^2\right) \\ & + P\left(\frac{rk}{(P+c)} + \gamma R - \mu_1\right) - \frac{\beta SP(1+\omega)}{1+b(1+\omega)S}\end{aligned}$$

After applying condition (15), the subsequent outcome is as follows:

$$\begin{aligned}\frac{dB_2}{dt} \leq & -\left(\sqrt{\mu_0}(S-S_2) + \sqrt{\frac{r}{2(P+c)}}P\right)^2 - \left(\sqrt{\mu_2}(R-R_2) + \sqrt{\frac{r}{2(P+c)}}P\right)^2 \\ & + P\left(\frac{rk}{(P+c)} + \gamma R - \mu_1\right) - \frac{\beta SP(1+\omega)}{1+b(1+\omega)S}.\end{aligned}$$

Then, ${}^{dB_2}/_{dt}$ under condition (15). Therefore, any solution starting from ϑ_2 approach asymptotically to H_2. □

Theorem 5
The basin of attraction of the revegetation-free point $H_3 = (S_3, \mathrm{P}_3,\ 0)$ is the sub-region of $\vartheta_3 \subset R_+^3$ which satisfies the following condition:

$$\left.\begin{array}{c}\sigma_2^2 \leq \sigma_1\sigma_3 \\ \frac{rc\left(P_3^2-P^2\right)(P-P_3)}{k(P+c)(P_3+c)} + \gamma RP + ek \leq \mu_2 R\end{array}\right\} \tag{16}$$

Proof
Define $B_3 = \frac{(S-S_3)^2}{2} + \left(P - P_3 - P_3 ln\frac{P}{P_3}\right) + R$, where B_3 is a positive definite function about H_3. Thus, $\frac{dB_3}{dt} = (S-S_3)\frac{dS}{dt} + \frac{(P-P_3)}{P}\frac{dP}{dt} + \frac{dR}{dt}$ i.e.,

$$\begin{aligned}\frac{dB_3}{dt} = & (S-S_3)\left[A - \mu_0 S - \frac{\alpha(1+\omega)SP}{1+b(1+\omega)S} - A + \mu_0 S_3 + \frac{\alpha(1+\omega)S_3P_3}{1+b(1+\omega)S_3}\right] \\ & + \frac{(P-P_3)}{P}\left[P\left(\frac{rkP - rP^2}{k(P+c)} - \frac{\beta(1+\omega)S}{1+b(1+\omega)S} + \gamma R - \mu_1\right) - \left(\frac{rkP_3 - rP_3^2}{k(P_3+c)} - \frac{\beta(1+\omega)S_3}{1+b(1+\omega)S_3} - \mu_1\right)\right] \\ & + [e(k-P) - \mu_2 R]\end{aligned}$$

Therefore,

$$\begin{aligned}\frac{dB_3}{dt} = & -\left(\sigma_1(S-S_3)^2 + \sigma_2(S-S_3)(P-P_3) + \sigma_2(P-P_3)^2\right) \\ & + \left(\frac{rc\left(P_3^2-P^2\right)(P-P_3)}{k(P+c)(P_3+c)} + \gamma RP + ek - \mu_2 R\right) - \gamma RP_3 - eP,\end{aligned}$$

where

$$\sigma_1 = \mu_0 + \frac{\alpha P_3(1+\omega)}{[1+b(1+\omega)S][1+b(1+\omega)S_3]}, \sigma_2 = \left(\frac{(1+\omega)[S\alpha + bSS_3\alpha(1+\omega) + \beta]}{[1+b(1+\omega)S][1+b(1+\omega)S_3]}\right),$$

and

$$\sigma_3 = \frac{r(PP_3 - ck)}{k(P+c)(P_3+c)}.$$

After applying condition (16), the subsequent outcome is as follows:

$$\frac{dB_3}{dt} \leq -\left(\sqrt{\sigma_1}\left(S-S_3\right)+\sqrt{\sigma_3}\left(P-P_3\right)\right)^2+\left(\frac{rc\left(P_3^2-P^2\right)\left(P-P_3\right)}{k\left(P+c\right)\left(P_3+c\right)}+\gamma RP+ek-\mu_2 R\right)-\gamma RP_3-eP.$$

Then, ${}^{dB_3}/_{dt}$. Therefore, any solution starting from ϑ_3 approach asymptotically to H_3. □

Theorem 6
The basin of attraction of the coexistence point $H_4=(S_4,\mathrm{P}_4,R_4)$ is the sub-region of $\vartheta_4\subset R_+^3$ which satisfies the following condition:

$$\left.\begin{array}{c}\epsilon_3\geq \max\left\{\frac{\epsilon_2^2}{\epsilon_1},\frac{(\gamma-e)^2}{\mu_2}\right\}\\ P_4^2P<P_4^3+P^3+P^2P_4\end{array}\right\} \tag{17}$$

Proof
Define $B_4=\frac{(S-S_4)^2}{2}+\left(P-P_4-P_4ln\frac{P}{P_4}\right)+\frac{(R-R_4)^2}{2}$, where B_4 is a positive definite about H_4. Thus, $\frac{dB_4}{dt}=\left(S-S_4\right)\frac{dS}{dt}+\frac{(P-P_4)}{P}\frac{dP}{dt}+\left(R-R_4\right)\frac{dR}{dt}$. i.e.,

$$\begin{aligned}\frac{dB_4}{dt}=&\left(S-S_4\right)\left[A-\mu_0S-\frac{\alpha\left(1+\omega\right)SP}{1+b\left(1+\omega\right)S}-A+\mu_0S_4+\frac{\alpha\left(1+\omega\right)S_4P_4}{1+b\left(1+\omega\right)S_4}\right]\\&+\frac{\left(P-P_4\right)}{P}\left[P\left(\frac{rkP-rP^2}{k\left(P+c\right)}-\frac{\beta\left(1+\omega\right)S}{1+b\left(1+\omega\right)S}+\gamma R-\mu_1\right)\right.\\&\left.-\left(\frac{rkP_4-rP_4^2}{k\left(P_4+c\right)}-\frac{\beta\left(1+\omega\right)S_4}{1+b\left(1+\omega\right)S_4}+\gamma R_4-\mu_1\right)\right]\\&+\left(R-R_4\right)\left[ek-eP-\mu_2R-ek+eP_4+\mu_2R_4\right]\end{aligned}$$

Therefore,

$$\begin{aligned}\frac{dB_4}{dt}=&-\left(\epsilon_1\left(S-S_4\right)^2-\epsilon_2\left(P-P_4\right)\left(S-S_4\right)-\epsilon_3\left(P-P_4\right)^2\right)\\&-\left(\epsilon_3\left(P-P_4\right)^2-\left(\gamma-e\right)\left(P-P_4\right)\left(R-R_4\right)+\mu_2\left(R-R_4\right)^2\right)\\&+\frac{rc\left(P_4^2P-P^2P_4-P_4^3-P^3\right)}{k\left(P+c\right)\left(P_4+c\right)}\end{aligned}$$

where

$$\epsilon_1=\mu_0+\frac{\alpha P_4\left(1+\omega\right)}{\left[1+b\left(1+\omega\right)S\right]\left[1+b\left(1+\omega\right)S_4\right]},\epsilon_2=\frac{\left(1+\omega\right)\left[\alpha S+bSS_4\alpha\left(1+\omega\right)+\beta\right.}{\left[1+b\left(1+\omega\right)S\right]\left[1+b\left(1+\omega\right)S_4\right]},$$

and

$$\epsilon_3=\frac{r\left(PP_4-ck\right)}{2k\left(P+c\right)\left(P_4+c\right)}.$$

After applying condition (17), the subsequent outcome is as follows:

$$\frac{dB_4}{dt}\leq-\left(\sqrt{\epsilon_1}\left(S-S_4\right)+\sqrt{\epsilon_3}\left(P-P_4\right)\right)^2-\left(\sqrt{\epsilon_3}\left(P-P_4\right)+\sqrt{\mu_2}\left(R-R_4\right)\right)^2+\frac{rc\left(P_4^2P-P_4^3-P^3-P^2P_4\right)}{k\left(P+c\right)\left(P_4+c\right)}.$$

Then, ${}^{dB_4}/_{dt}$ under condition (17). Therefore, any solution starting from ϑ_4 approach asymptotically to H_4. □

7. Local bifurcation

This section investigates some types of bifurcation, such as saddle-node, transcritical, and Hopf bifurcation, occurring in the vicinity of non-hyperbolic equilibrium points [25, 26]. The SPR system can be expressed in the following forms to assist in this determination:

$$\frac{dH}{dt} = F(H), \text{ where } H = \begin{pmatrix} S \\ P \\ R \end{pmatrix}, \text{ and } F = \begin{pmatrix} f_1(S,P) \\ f_2(S,P,R) \\ f_3(P,R) \end{pmatrix}$$

Theorem 7
For $\beta^* = \frac{(\gamma R_2 - \mu_1)[1+bS_1(1+\omega)]}{S_1(1+\omega)}$, the SPR model, at H_2 has a TB if

$$\frac{\beta^* C_1^{[2]}(1+\omega)}{[1+bS_2(1+\omega)]^2} \neq \gamma C_3^{[2]}. \tag{18}$$

Proof
At $\beta^* = \frac{(\gamma R_2 - \mu_1)[1+bS_1(1+\omega)]}{S_1(1+\omega)}$, $J(H_2)$ has a zero eigenvalue $\lambda_2^0 = 0$. So, $J(S_2)$ at β^* becomes

$$J^*(H_2) = \begin{bmatrix} -\mu_0 & \frac{-\alpha S_2(1+\omega)}{1+bS_2(1+\omega)} & 0 \\ 0 & 0 & 0 \\ 0 & -e & -\mu_2 \end{bmatrix}$$

Now, suppose that

$$C^{[2]} = \left(C_1^{[2]}, C_2^{[2]}, C_3^{[2]}\right)^T,$$

and

$$W^{[2]} = \left(W_1^{[2]}, W_2^{[2]}, W_3^{[2]}\right)^T$$

be eigenvectors to $\lambda_2^0 = 0 of J^*(H_2)$ and $J^{*T}(H_2)$, respectively. The computation gives

$$C^{[2]} = \left(\frac{-\alpha S_2(1+\omega)}{1+bS_2(1+\omega)}, 1, \frac{-e}{\mu_2}\right)^T$$

and $W^{[2]} = (0, 1, 0)^T$ by solving $(J^*(H_2) - \lambda_2^0 I)C^{[2]}$, and $(J^{*T}(H_2) - \lambda_2^0 I)W^{[2]} for C^{[2]}$ and $W^{[2]}$.
Now,

$$\frac{dF}{d\beta} = F_\beta(H,\beta) = \left(\frac{df_1}{d\beta}, \frac{df_2}{d\beta}, \frac{df_3}{d\beta}\right) = \left(0, \frac{-(1+\omega)SP}{1+b(1+\omega)S}, 0\right) \Rightarrow F_\beta(H_2, \beta^*) = (0,0,0).$$

Hence,

$$W^{[2]^T} F_\beta(H_2, \beta^*) = (0,1,0)\begin{pmatrix} 0 \\ 0 \\ 0 \end{pmatrix} = 0.$$

Subsequently,

$$W^{[2]^T}\left[DF_\beta(H_2,\beta^*)C^{[2]}\right] = (0,1,0)\begin{bmatrix} 0 & 0 & 0 \\ 0 & \frac{-(1+\omega)S_2}{1+b(1+\omega)S_2} & 0 \\ 0 & 0 & 0 \end{bmatrix}\begin{bmatrix} \frac{-\alpha S_2(1+\omega)}{\mu_0 + bS_2(1+\omega)\mu_0} \\ 1 \\ \frac{-e}{\mu_2} \end{bmatrix} = \frac{-(1+\omega)S_2}{1+b(1+\omega)S_2} \neq 0.$$

$$W^{[2]^T}\left[D^2F_\beta(H_2,\beta^*)(C^{[2]},C^{[2]})\right] = (0,1,0)\begin{bmatrix} \frac{-2\alpha C_1^{[2]}(1+\omega)}{[1+bS_2(1+\omega)]^2} \\ \frac{-2\beta^* C_1^{[2]}(1+\omega)}{[1+bS_2(1+\omega)]^2} + 2\gamma C_3^{[2]} \\ 0 \end{bmatrix} = 2\gamma C_3^{[2]} - \frac{2\beta^* C_1^{[2]}(1+\omega)}{[1+bS_2(1+\omega)]^2}$$

Therefore, there is a TB around H_2 with the parameter β^* if condition (18) is satisfied. □

Theorem 8
The SPR system faces a Hopf bifurcation at H_4 arond α^* if

$$Z_i > 0, i = 1, 2, \tag{19}$$

$$\Theta(\alpha^*)\psi(\alpha^*) + \Gamma(\alpha^*)\phi(\alpha^*) \neq 0, \tag{20}$$

where $Z_i,\ i = 1, 2$ are stated in (13) with $\alpha = \alpha^*$.

Proof
The Hopf bifurcation α^* could be found if we set $Z_1(\alpha^*)Z_2(\alpha^*) - Z_3(\alpha^*) = 0$. Then, at $\alpha = \alpha^*$, Eq. (13) can be written as

$$(\lambda + Z_1)\left(\lambda^2 + Z_2\right) = 0.$$

Then, the following roots are obtained

$$\lambda_1 = -Z_1 \text{ and } \lambda_{2,3} = \pm i\sqrt{Z_2}$$

Clearly $\lambda_1 < 0$, and $\lambda_{2,3}$ are two purely imaginary roots if condition (19) is met. While in the neighbourhood of $\alpha^*, \lambda_{2,3}$ have the forms: $\lambda_1 = -Z_1, \lambda_{2,3} = \delta_1(\alpha) \pm i\delta_2(\alpha)$. The following conditions are now considered to signify the occurrence of HB at $\alpha = \alpha^*$.

1. $Re(\lambda_{2,3})|_{\alpha=\alpha^*} = \delta_1(\alpha^*) = 0$.
2. We substitute$\delta_1(\alpha) \pm i\delta_2(\alpha)$ into (13), to compute the transversality condition, $\Theta(\alpha^*)\psi(\alpha^*) + \Gamma(\alpha^*)\phi(\alpha^*) \neq 0$, where $\Theta(\alpha), \psi(\alpha), \Gamma(\alpha)$, and $\phi(\alpha)$ are

$$\begin{aligned}
\psi(\alpha) &= 3\delta_1^2(\alpha) + 2Z_1(\alpha)\delta_1(\alpha) + Z_2(\alpha) - 3\delta_2^2(\alpha),\\
\phi(\alpha) &= 6\delta_1(\alpha)\delta_2(\alpha) + 2Z_1(\alpha)\delta_2(\alpha),\\
\Theta(\alpha) &= \delta_1^2(\alpha)Z_1\prime(\alpha) + Z_2\prime(\alpha)\delta_1(\alpha) + Z_3\prime(\alpha) - Z_1\prime(\alpha)\delta_2^2(\alpha),\\
\Gamma(\alpha) &= 2\delta_1(\alpha)\delta_2(\alpha)Z_1\prime(\alpha) + Z_2\prime(\alpha)\delta_2(\alpha).
\end{aligned}$$

Now at $\alpha = \alpha^*$, substitution $\delta_1 = 0$ and $\delta_2 = \sqrt{Z_2}$, the following is obtained:

$$\begin{aligned}
\psi(\alpha^*) &= -2Z_2(\alpha^*),\\
\phi(\alpha^*) &= 2Z_1(\alpha^*)\sqrt{Z_2(\alpha^*)},\\
\Theta(\alpha^*) &= Z_3'(\alpha^*) - Z_1'(\alpha^*)Z_2(\alpha^*),\\
\Gamma(\alpha^*) &= Z_2'(\alpha^*)\sqrt{Z_2(\alpha^*)},
\end{aligned}$$

where

$$Z_1'(\alpha^*) = \frac{P_4(1+\omega)}{[1+bS_4(1+\omega)]^2}$$

$$Z_2'(\alpha^*) = -\left(\frac{P_4(1+\omega)}{[1+bS_4(1+\omega)]^2}\right)\left(\frac{rP_4\left(ck - 2cP_4 - P_4^2\right)}{k(P_4+c)^2}\right) + \frac{P_4(1+\omega)\mu_2}{[1+bS_4(1+\omega)]^2} - \frac{\beta P_4 S_4(1+\omega)^2}{[1+bS_4(1+\omega)]^3}.$$

$$Z_3'(\alpha^*) = \left(\frac{\mu_2 P_4(1+\omega)}{[1+bS_4(1+\omega)]^2}\right)\left(\frac{rP_4\left(ck - 2cP_4 - P_4^2\right)}{k(P_4+c)^2}\right) + \frac{e\gamma P_4^2(1+\omega)}{[1+bS_4(1+\omega)]^2} - \frac{\beta P_4 S_4(1+\omega)^2\mu_2}{[1+bS_4(1+\omega)]^3}.$$

Hence, condition (20) gives

$$\Theta(\alpha^*)\psi(\alpha^*) + \Gamma(\alpha^*)\phi(\alpha^*) = -2Z_2(\alpha^*)\left(Z_3'(\alpha^*) - Z_1'(\alpha^*)Z_2(\alpha^*)\right) + 2Z_1(\alpha^*)Z_2'(\alpha^*)Z_2(\alpha^*) \neq 0$$

under condition (20). So, the HB has occurred at α^*.
The coefficient of curvature of the limit cycle is employed to present the stability condition of the stable limit cycle in $R^3_{(S,P,R)}$ from Theorem 9. We refer to [27] for a more detailed discussion.

□

Theorem 9
If

$$\frac{(1+\omega)U_1}{16{U_2}^2}\left(\beta-\frac{U_4}{{U_2}^2}\right)U_3+\frac{bU_1(1+\omega)^2}{8{U_2}^3}(3U_1U_4-\beta)<\left(\frac{(1+\omega)U_1U_4}{16{U_2}^2}\right)\left(U_3+\frac{\alpha U_1(1+\omega)}{{U_2}^2}\right). \quad (21)$$

Then, SPR model has a stable limit cycle in $R^3_{(S,P,R)}$

Proof
The following transformations $S=S^*+S_4, P=P^*+P_4, R=R^*+R_4$ is used to shift $S_4(S_4,P_4,R_4)$ to $(0,0,0)$. Then, the SPR system becomes:

$$\begin{aligned}
\frac{dS^*}{dt}&=A-\frac{\alpha(1+\omega)(S^*P^*)}{1+b(1+\omega)(S^*+S_4)}-\mu_1(S^*+S_4)\\
\frac{dP^*}{dt}&=r(P^*+P_4)+\frac{rkP^{*2}-rP^{*3}-3rP_4P^{*2}}{k(P^*+P_4)+c}-\frac{\beta(1+\omega)(S^*P^*)}{1+b(1+\omega)(S^*+S_4)}+\gamma(P^*R^*)-\mu_2(P^*+P_4)\\
\frac{dR^*}{dt}&=e(k-(P^*+P_4))-\mu_3(R^*+R_4).
\end{aligned}$$

The nonlinear component of the system above can be expressed as

$$\omega=\begin{bmatrix}\omega_1\\ \omega_2\\ \omega_3\end{bmatrix}=-\begin{bmatrix}\frac{\alpha(1+\omega)(S^*P^*)}{1+b(1+\omega)(S^*+S_4)}\\ \frac{(3rP_4-rk)P^{*2}+rP^{*3}}{k(P^*+P_4)+c}+\frac{\beta(1+\omega)(S^*P^*)}{1+b(1+\omega)(S^*+S_4)}-\gamma(P^*R^*)\\ 0\end{bmatrix}.$$

Then, the following quantities are derived.

$$\begin{aligned}
g^0_{20}=&\frac{1}{4}\left\{\frac{\partial^2\omega_1}{\partial{S^*}^2}-\frac{\partial^2\omega_1}{\partial{P^*}^2}+2\frac{\partial^2\omega_2}{\partial S^*\partial P^*}+i\left(\frac{\partial^2\omega_2}{\partial{S^*}^2}-\frac{\partial^2\omega_2}{\partial{P^*}^2}-2\frac{\partial^2\omega_1}{\partial S^*\partial P^*}\right)\right\}\\
=&\frac{1}{4}\left\{\frac{-2\alpha bP^*(1+\omega)^2[1+bS_4(1+\omega)]}{[1+b(1+\omega)(S^*+S_4)]^3}+\frac{2\beta(1+\omega)(1+bS_4(1+\omega))}{[1+b(1+\omega)(S^*+S_4)]^2}\right.\\
&+i\left(\frac{-2\beta bP^*(1+\omega)^2(1+bS_4(1+\omega))}{[1+b(1+\omega)(S^*+S_4)]^3}+\frac{4rk^2P^{*3}+v_1P^{*2}+v_2P^*+v_3}{[k(P^*+P_4)+c]^3}\right.\\
&\left.\left.-\frac{2\alpha(1+\omega)[1+bS_4(1+\omega)]}{[1+b(1+\omega)(S^*+S_4)]^2}\right)\right\}
\end{aligned}$$

$$\begin{aligned}
g^0_{11}=&\frac{1}{4}\left\{\frac{\partial^2\omega_1}{\partial{S^*}^2}+\frac{\partial^2\omega_1}{\partial{P^*}^2}+i\left(\frac{\partial^2\omega_2}{\partial{S^*}^2}+\frac{\partial^2\omega_2}{\partial{P^*}^2}\right)\right\}\\
=&\frac{1}{4}\left\{\frac{-2\alpha bP^*(1+\omega)^2[1+bS_4(1+\omega)]}{[1+b(1+\omega)(S^*+S_4)]^3}+i\left(\frac{-2\beta bP^*(1+\omega)^2(1+bS_4(1+\omega))}{[1+b(1+\omega)(S^*+S_4)]^3}\right.\right.\\
&\left.\left.+\frac{4rk^2P^{*3}+v_1P^{*2}+v_2P^*+v_3}{[k(P^*+P_4)+c]^3}\right)\right\}
\end{aligned}$$

$$G_{110}^0 = \frac{1}{2}\left\{\frac{\partial^2\omega_1}{\partial S^*\partial R^*} + \frac{\partial^2\omega_2}{\partial P^*\partial R^*} + i\left(\frac{\partial^2\omega_2}{\partial S^*\partial R^*} - \frac{\partial^2\omega_1}{\partial P^*\partial R^*}\right)\right\} = -\frac{\gamma}{2}.$$

$$G_{101}^0 = \frac{1}{2}\left\{\frac{\partial^2\omega_1}{\partial S^*\partial R^*} - \frac{\partial^2\omega_2}{\partial P^*\partial R^*} + i\left(\frac{\partial^2\omega_2}{\partial S^*\partial R^*} + \frac{\partial^2\omega_1}{\partial P^*\partial R^*}\right)\right\} = \frac{\gamma}{2}.$$

$$W_{11}^0 = -\frac{1}{4\lambda_3(a_1(k^*)}\left(\frac{\partial^2\omega_3}{\partial {S^*}^2} + \frac{\partial^2\omega_3}{\partial {P^*}^2}\right) = 0.$$

$$W_{20}^0 = -\frac{1}{4\lambda_3(a_1(k^*)}\left(\frac{\partial^2\omega_3}{\partial {S^*}^2} + \frac{\partial^2\omega_3}{\partial {P^*}^2} - 2i\frac{\partial^2\omega_3}{\partial S^*\partial R^*}\right) = 0.$$

$$\begin{aligned} G_{21}^0 =& \frac{1}{8}\left\{\frac{\partial^3\omega_1}{\partial {S^*}^3} + \frac{\partial^3\omega_1}{\partial S^*\partial {P^*}^2} + \frac{\partial^3\omega_2}{\partial {P^*}^3} + \frac{\partial^3\omega_2}{\partial {S^*}^2\partial P} + i\left(\frac{\partial^3\omega_2}{\partial {S^*}^3} + \frac{\partial^3\omega_2}{\partial S^*\partial {P^*}^2} - \frac{\partial^3\omega_1}{\partial {P^*}^3} - \frac{\partial^3\omega_1}{\partial {S^*}^2\partial P}\right)\right\} \\ =& \frac{1}{8}\left\{\frac{6\alpha b^2P^*\left(1+\omega\right)^3\left[1+bS_4\left(1+\omega\right)\right]}{\left[1+b\left(1+\omega\right)\left(S^*+S_4\right)\right]^4} + \frac{v_4{P^*}^2+v_5P^*+v_6}{\left[k\left(P^*+P_4\right)+c\right]^4} - \frac{2\beta b\left(1+\omega\right)^2\left(1+bS_4\left(1+\omega\right)\right)}{\left[1+b\left(1+\omega\right)\left(S^*+S_4\right)\right]^3}\right. \\ &\left. + i\left(\frac{6\beta b^2P^*\left(1+\omega\right)^3\left(1+bS_4\left(1+\omega\right)\right)}{\left[1+b\left(1+\omega\right)\left(S^*+S_4\right)\right]^4} - \frac{-2\alpha b\left(1+\omega\right)^2\left[1+bS_4\left(1+\omega\right)\right]}{\left[1+b\left(1+\omega\right)\left(S^*+S_4\right)\right]^3}\right)\right\} \end{aligned}$$

The coefficient of the curvature of the limit cycle of the SPR system is

$$\chi_1^0 = Re\left\{\frac{g_{20}^0g_{11}^0}{4}i + G_{110}^0W_{11}^0 + \frac{G_{21}^0 + G_{101}^0W_{20}^0}{2}\right\}$$

$$\begin{aligned} \chi_1^0 =& Re\left\{\frac{\left(1+\omega\right)U_1}{16{U_2}^2}\left(\beta - \frac{\alpha bP^*\left(1+\omega\right)}{{U_2}^3}\right)\left(\frac{\beta bP^*\left(1+\omega\right)^2U_1}{{U_2}^3} - \frac{4rk^2{P^*}^3+v_1{P^*}^2+v_2P^*+v_3}{2\left[k\left(P^*+P_4\right)+c\right]^3}\right)\right. \\ &- \left(\frac{\alpha bP^*\left(1+\omega\right)^2U_1}{16{U_2}^3}\right)\left(\frac{\beta bP^*\left(1+\omega\right)^2U_1}{{U_2}^3} - \frac{4rk^2{P^*}^3+v_1{P^*}^2+v_2P^*+v_3}{2\left[k\left(P^*+P_4\right)+c\right]^3} + \frac{\alpha U_1\left(1+\omega\right)}{{U_2}^2}\right) \\ &+ \frac{bU_1\left(1+\omega\right)^2}{8{U_2}^3}\left(\frac{3\alpha bP^*\left(1+\omega\right)U_1}{U_2} - \beta\right) + \left(\frac{6\beta b^2P^*\left(1+\omega\right)^3U_1}{{U_2}^4} + \frac{2\alpha b\left(1+\omega\right)^2U_1}{{U_2}^3}\right)i \\ &+ \left(\frac{-2\alpha bP^*\left(1+\omega\right)^2U_1}{{U_2}^3} + \frac{2\beta\left(1+\omega\right)U_1}{{U_2}^2}\right)\left(\frac{-2\alpha bP^*\left(1+\omega\right)^2U_1}{{U_2}^3}\right)i \\ &+ \left(\frac{2\beta bP^*\left(1+\omega\right)^2U_1}{{U_2}^3} - \frac{4rk^2{P^*}^3+v_1{P^*}^2+v_2P^*+v_3}{\left[k\left(P^*+P_4\right)+c\right]^3}\right) \\ &\left.\left(\frac{-2\beta bP^*\left(1+\omega\right)^2U_1}{{U_2}^3} + \frac{4rk^2{P^*}^3+v_1{P^*}^2+v_2P^*+v_3}{\left[k\left(P^*+P_4\right)+c\right]^3} - \frac{2\alpha\left(1+\omega\right)U_1}{{U_2}^2}\right)i\right\}. \end{aligned}$$

$$\Longrightarrow \chi_1^0 = \frac{\left(1+\omega\right)U_1}{16{U_2}^2}\left(\beta - \frac{U_4}{{U_2}^2}\right)U_3 + \frac{bU_1\left(1+\omega\right)^2}{8{U_2}^3}\left(3U_1U_4 - \beta\right) - \left(\frac{\left(1+\omega\right)U_1U_4}{16{U_2}^2}\right)\left(U_3 + \frac{\alpha U_1\left(1+\omega\right)}{{U_2}^2}\right),$$

where,

$$U_1 = 1 + bS_4\left(1+\omega\right), U_2 = 1 + b\left(1+\omega\right)\left(S^*+S_4\right), U_3 = \frac{\beta bP^*\left(1+\omega\right)^2U_1}{{U_2}^3} - \frac{4rk^2{P^*}^3+v_1{P^*}^2+v_2P^*+v_3}{2\left[k\left(P^*+P_4\right)+c\right]^3},$$

and

$$U_4 = \frac{\alpha bP^*\left(1+\omega\right)}{U_2}.$$

Thus, $\chi_1^0 < 0$ under condition (21); hence, the SPR model has a stable limit cycle, indicating a supercritical Hopf bifurcation. □

8. Numerical simulation and discussion

The numerical simulation of the Dust-Plant-Revegetation (SPR) model was conducted using the parameter values provided in Table 1. To solve the system numerically, the classical fourth-order Runge–Kutta method was employed, with a fixed step size $h = 0.001$ and with the initial condition $(S_0, P_0, R_0) = (5.2, 8.3, 15.2)$. We first present the phase portrait and time series of our proposed system in Figures 3 and 4, respectively. Figure 3 demonstrates that the system is stable around the interior equilibrium point, with all solution trajectories converging towards the basin of this stable equilibrium. Figure 4 illustrates a periodic oscillatory behavior in the state variables $S(t), P(t)$, and $R(t)$. This pattern indicates the existence of a limit cycle, where the system avoids reaching a steady state and instead experiences continuous oscillations over time. These two figures confirm that the system undergoes a Hopf bifurcation. In both cases, all elements persist in the system.

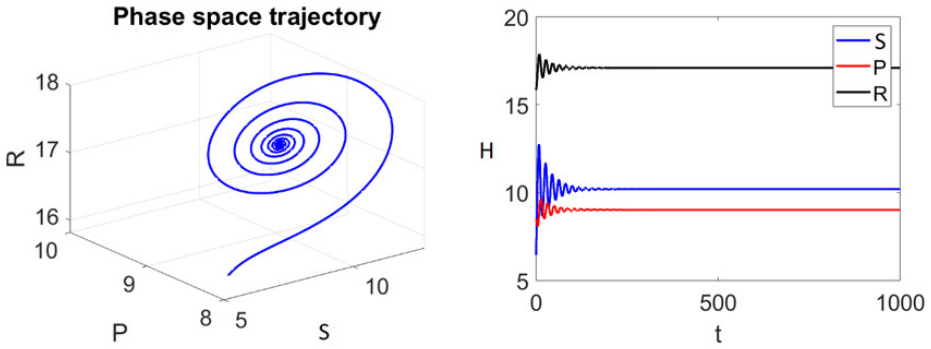

Figure 3. Phase portrait and time series of the SPR model with the parameters given in Table 1.

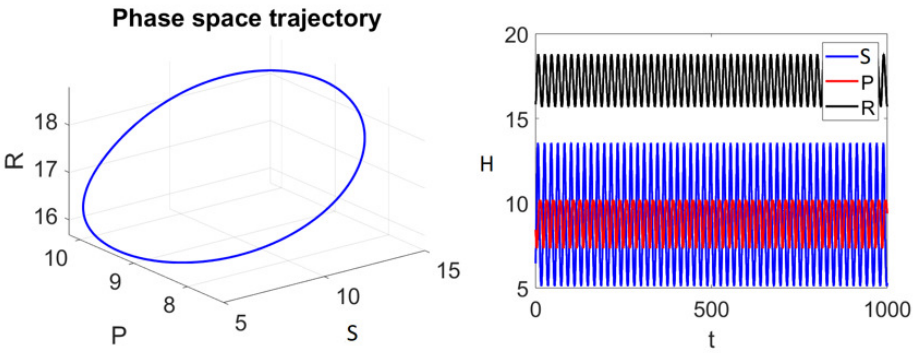

Figure 4. Phase portrait and time series of the SPR model with $\omega = 4.1$, and the remaining parameters are the same as those given in Table 1.

Now we analyze the dynamical behavior of the proposed model by varying the model parameter ω, which represents the effect of wind on dust dynamics. The phase space trajectories and time series plots illustrate a transition from stable equilibrium to chaotic dynamics through a sequence of bifurcations. At $\omega = 2.0$, the system converges to a stable equilibrium (See Figure 5a), where the phase space trajectory exhibits a spiral motion settling into a fixed point, and the time series plots show damped oscillations. As ω increases to 3.0, the system undergoes a Hopf bifurcation, leading to a stable periodic orbit, indicating sustained oscillations in dust, plant biomass, and revegetation levels (See Figure 5b). Further increasing ω to 4.2 results in a period-doubling bifurcation (See Figure 5c), where the system exhibits a two-period oscillation, suggesting fluctuations in plant biomass and revegetation

dynamics due to increased dust levels. At $\omega = 4.255$, another bifurcation occurs, producing a four-period oscillation (See Figure 6a), followed by an eight-period oscillation at $\omega = 4.31$ (See Figure 5b). As w reaches 5.0, the system enters a chaotic regime (See Figure 5c), characterized by a strange attractor in phase space and irregular, non-repeating oscillations in the time series. This sequence of bifurcations demonstrates a classical route to chaos via period-doubling, highlighting the significant role of wind effects in shaping the interactions between dust storms, plant biomass, and revegetation.

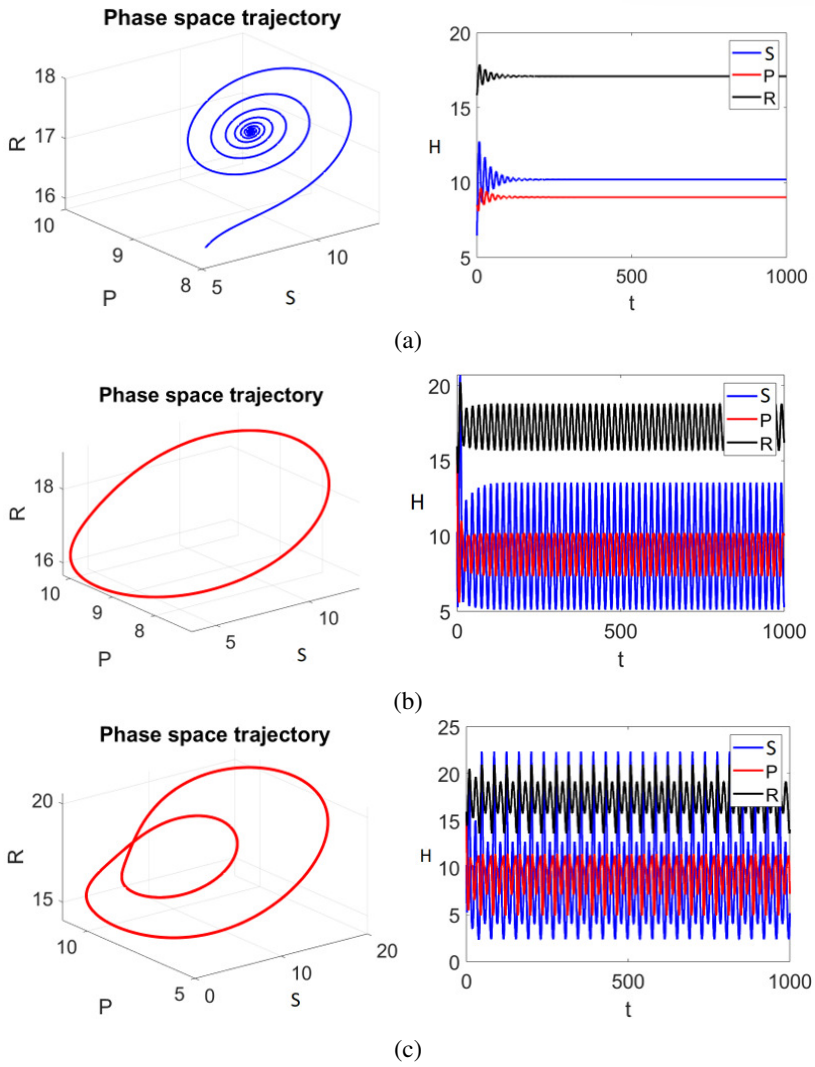

Figure 5. Phase portrait and time series of the SPR model with respect to ω: a) Coexistence within the system is possible when $\omega = 2$, b) A stable periodic orbit in the system is observed when $\omega = 3$, c) A two-period oscillation within the system is sustained when $\omega = 4.2$.

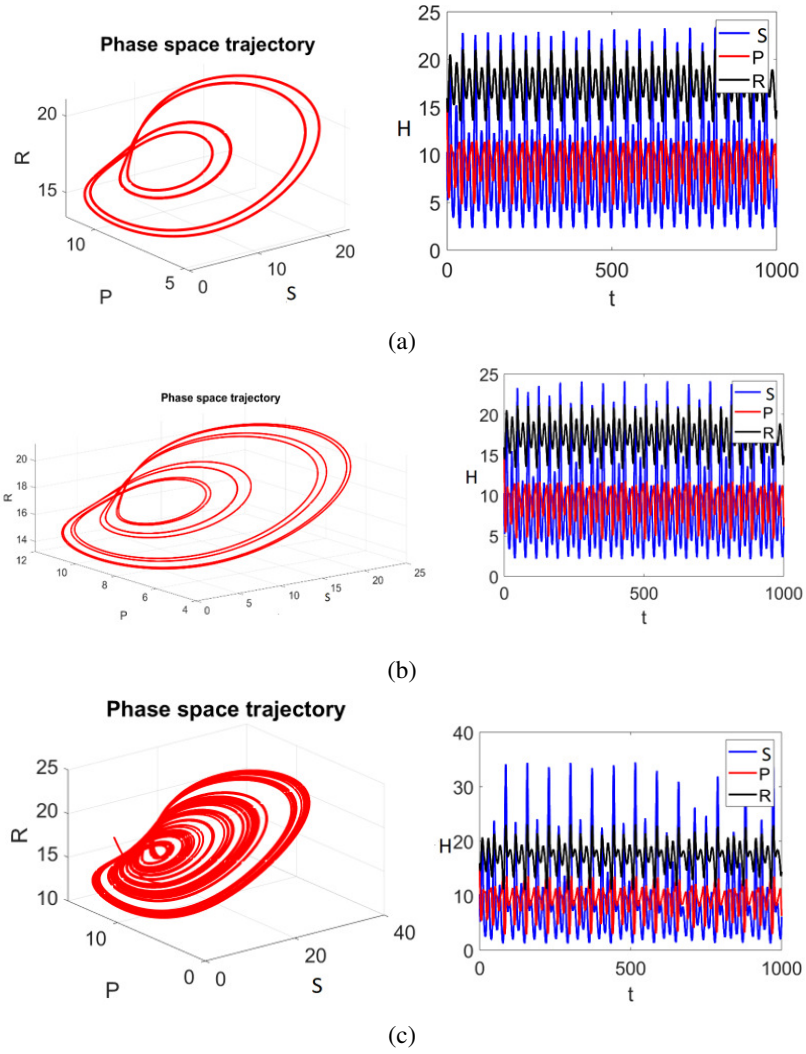

Figure 6. Phase portrait and time series of the SPR model with respect to ω: a) A four-period oscillation within the system is possible when $\omega = 4.255$, b) An eight-period oscillation in the system is observed when $\omega = 4.31$, c) An irregular (non-repeating) oscillation within the system is sustained when $\omega = 5$.

To explore potential mechanisms for controlling chaotic behavior, we investigate the influence of the parameter b, which represents the half-saturation level affecting dust-plant interactions. At b=0.2, the system exhibits chaotic dynamics (See Figure 7a), as evidenced by the presence of a strange attractor in the phase space trajectory and irregular, non-periodic oscillations in the time series. A slight increase to $b = 0.202$ leads to the emergence of a two-period oscillation (See Figure 7b), marking the onset of a period-doubling bifurcation. At $b = 0.204$, the system stabilizes into a limit cycle characterized by sustained periodic oscillations in dust accumulation, plant biomass growth, and revegetation activities (See Figure 7c). As b increases further to 0.22, the system undergoes a transition to a stable equilibrium(See Figure 8, where the phase space trajectory spirals toward a fixed point, and the time series plots show damped oscillations. This transition from chaos to stability through period-doubling bifurcations highlights the sensitivity of the SPR system to variations in b. The results suggest that adjusting the half-saturation level of dust depletion can effectively regulate chaotic dynamics in environmental management models. These insights are valuable for optimizing revegetation initiatives and mitigating dust storms's adverse effects on plant biomass sustainability.

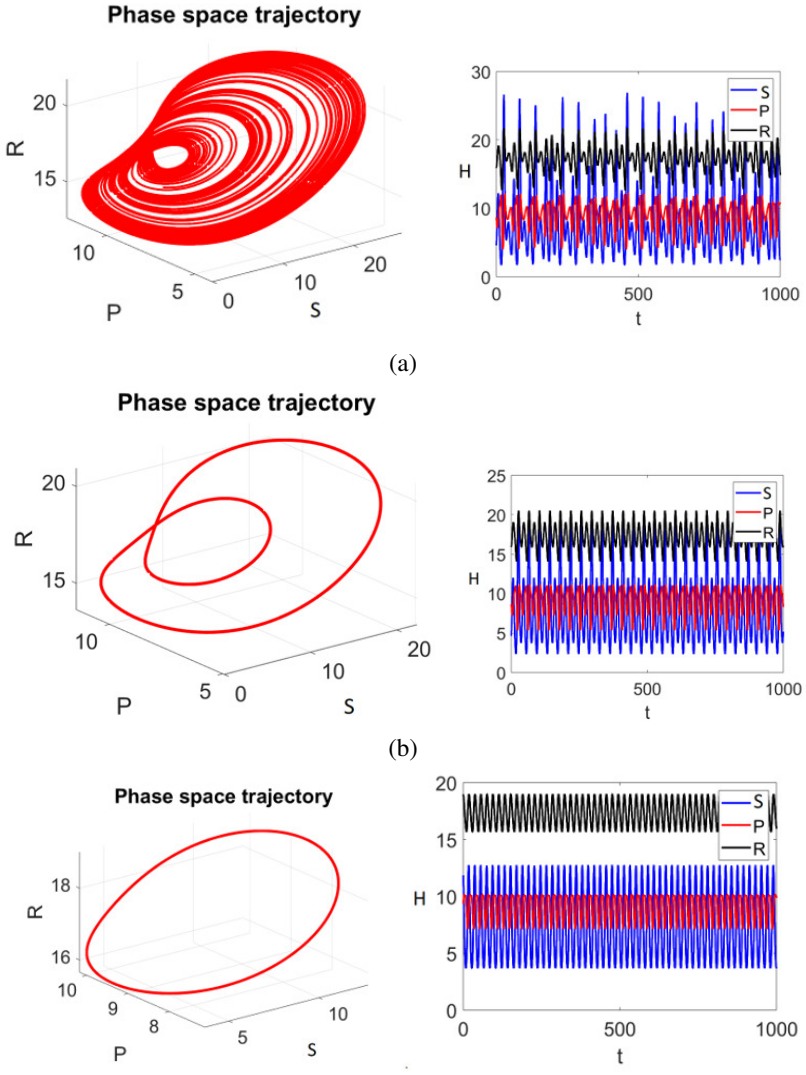

Figure 7. Phase portrait and time series of the SPR model with an increased value of b: a) Occurrence of a strange attractor in the system when the parameter $b = 0.2$, b) Occurrence of a two-period oscillation with $b = 0.202$, c) Occurrence of a limit cycle with $b = 0.204$.

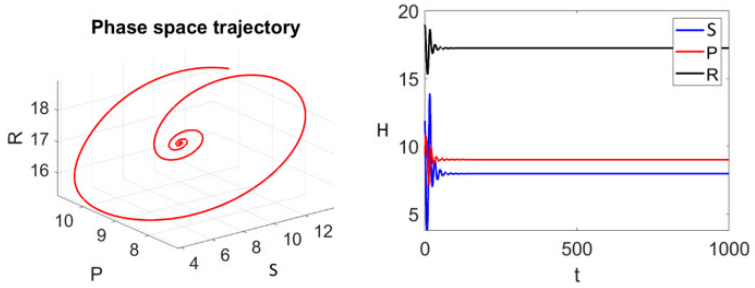

Figure 8. Coexistence within the SPR system is possible when the parameter $b = 0.22$.

The bifurcation diagrams illustrate how the system transitions from a stable equilibrium to periodic oscillations and, eventually, chaotic behavior as ω increases. The three figures correspond to the steady-state and long-term behavior of dust storms (S), plant biomass (P), and revegetation activities (R) as functions of ω.

The first bifurcation diagram (Figure 9) shows the variation of dust storms levels with increasing wind intensity. For small values of ω, S stabilizes, indicating a steady state where the dust accumulation and depletion balance each other. As ω increases beyond a critical threshold, a bifurcation occurs, leading to periodic oscillations in dust levels. Further increases in ω result in a sequence of period-doubling bifurcations, eventually driving the system into a chaotic regime. This chaotic behavior suggests unpredictable and highly sensitive dust storm dynamics under strong wind conditions. The coexistence of multiple branches (red and blue points) indicates bistability, where the system may settle into different long-term states depending on initial conditions.

The second Figure (Figure 9) presents the bifurcation structure of plant biomass. For low values of ω, plant biomass remains relatively stable, suggesting that wind effects do not significantly disrupt vegetation growth at lower intensities. However, as ω increases, the system undergoes a bifurcation, leading to periodic fluctuations in plant biomass. These fluctuations reflect the alternating phases of dust accumulation and removal, which influence plant growth; a series of period-doubling bifurcations occur, culminating in chaotic oscillations for larger values of ω. The coexistence of multiple branches at high w values suggests that plant biomass levels may experience significant variations depending on external disturbances and initial conditions.

The third bifurcation diagram (Figure 9) illustrates that at a low value of ω, it remains stable, indicating that revegetation activities are sufficient to balance plant depletion due to dust storms. However, as ω increases, a bifurcation occurs, leading to oscillatory behavior in revegetation dynamics. For moderate values of ω, these oscillations remain periodic, reflecting a balance between revegetation activities and plant biomass fluctuations. As ω surpasses a critical value, period-doubling bifurcations emerge, followed by chaotic dynamics at higher ω values. The presence of multiple stable states (red and blue points) highlights the system's sensitivity to wind effects, where slight changes in initial conditions or environmental factors can lead to drastically different long-term outcomes. The bifurcation analysis of the SPR model reveals that wind intensity (ω) plays a crucial role in shaping the stability and dynamics of dust storms, plant biomass, and revegetation activities. At low wind intensities, the system maintains stability with minimal fluctuations. However, as ω increases, periodic oscillations and chaotic dynamics emerge, indicating that strong wind effects can introduce unpredictability into the system. The observed bistability further suggests that similar environmental conditions can lead to vastly different outcomes based on initial states and external perturbations.

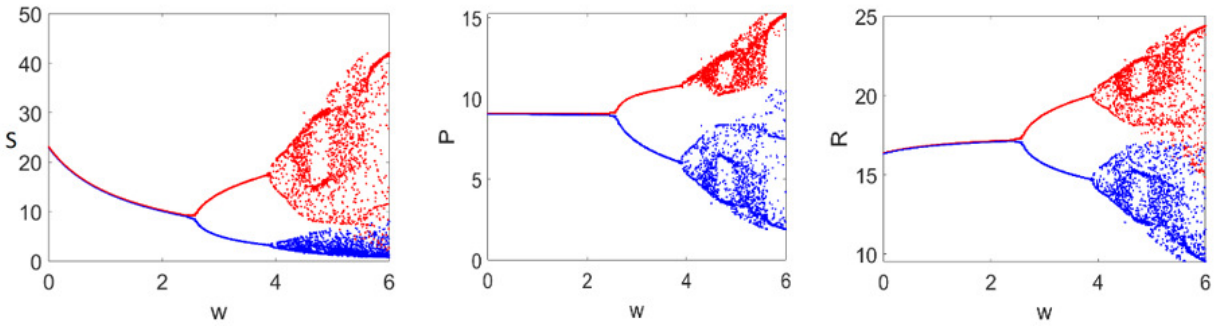

Figure 9. Bifurcation diagram w.r.t $\omega = 2.6$.

8.1. Two parametric bifurcation w.r.t $\alpha - \beta$ and $r - \alpha$.

The figures presented illustrate the two-parameter bifurcation diagrams for the Dust-Plant-Revegetation (SPR) model, depicting the impact of key parameters on system stability and transitions between different dynamical regimes. The diagrams identify GH bifurcation points, which indicate the presence of Generalized Hopf (GH) bifurcations, marking the transition from supercritical to subcritical Hopf bifurcations. These critical points highlight parameter regions where qualitative changes in system behavior occur.

This diagram (see Figure 10a) explores the effect of the depletion of dust pollutants owing to plant biomass (α) and the depletion rate of vegetation cover due to a dust storm (β) on system stability. The diagram is divided into two distinct regions: The blue curve represents the Hopf bifurcation boundary separating the stable and oscillatory regimes. As α and β increase, the system undergoes a Hopf bifurcation, transitioning from a steady state to oscillatory dynamics. The red stars labeled "GH" indicate Gavrilov-Guckenheimer bifurcations, where the nature of the Hopf bifurcation changes, leading to the emergence of more complex oscillatory behaviors.

Figure 10a examines the relationship between the (r) and (α). The GH bifurcation points marked by red stars represent critical parameter values where the Hopf bifurcation changes its nature, potentially leading to the onset of complex oscillations. The presence of these bifurcations suggests that small changes in r or α can lead to significant alterations in system behavior, influencing the long-term stability of vegetation and dust dynamics.

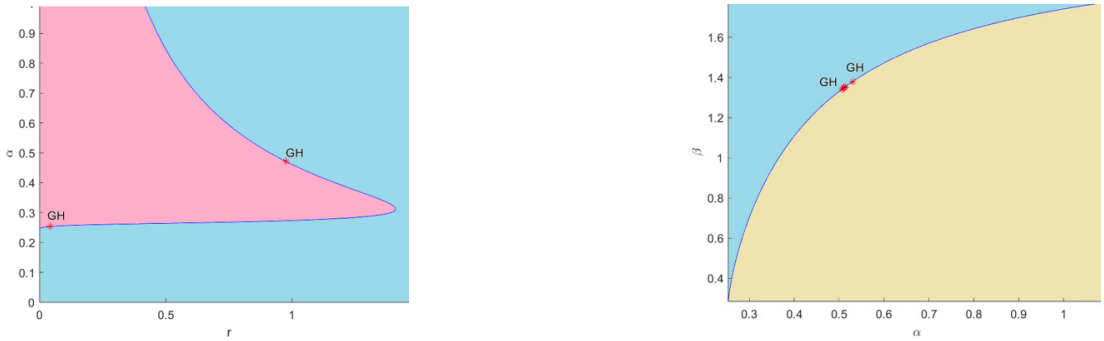

(a) (b)

Figure 10. Two-parametric Bifurcation diagram.

The dynamical response of the SPR model, governed by Eqs. (1)–(**??**), may shift toward generating sustained oscillations around its interior equilibrium. These oscillations, reflecting recurrent variations in dust concentration, vegetation cover, and restoration activity, are determined by the Jacobian matrix of the system. First, at a critical value of the revegetation implementation rate (e), the system undergoes a Hopf bifurcation, leading to a qualitative change in stability and the emergence of limit cycles (Figure 11a). Second, an analogous bifurcation occurs at a threshold value of the restoration-induced biomass growth rate (γ), where the same mathematical conditions are satisfied, again giving rise to sustained oscillations (Figure 11b). Thus, either parameter, when tuned to its critical level, can serve as the bifurcation driver that destabilizes the equilibrium and initiates cyclic dynamics.

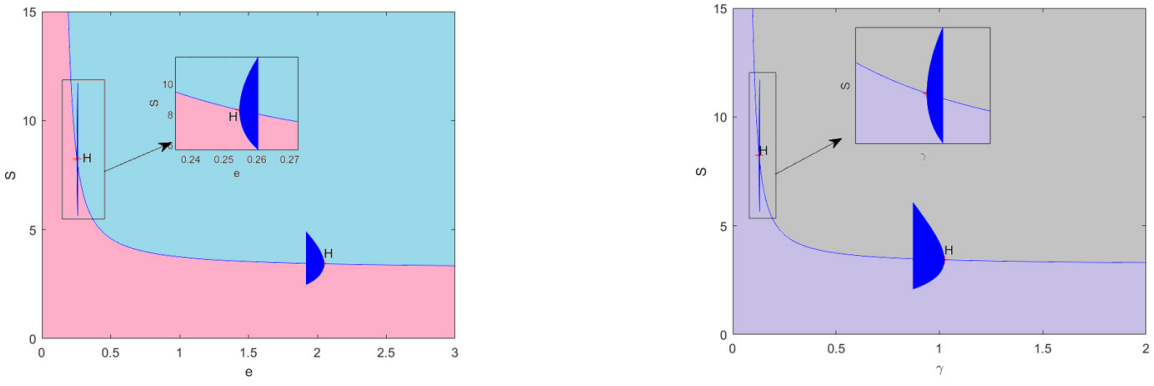

(a) (b)

Figure 11. One-parameter Bifurcation w.r.to e and γ.

We display the phase portrait and time series of the system for different values of A in Figure 12. The results show that the system is initially stable, then becomes periodic as A increases the value, and finally returns to a stable state at higher values of A. Figure 13 shows that as the value of μ_0 increases, the system changes from a stable state to a periodic one.

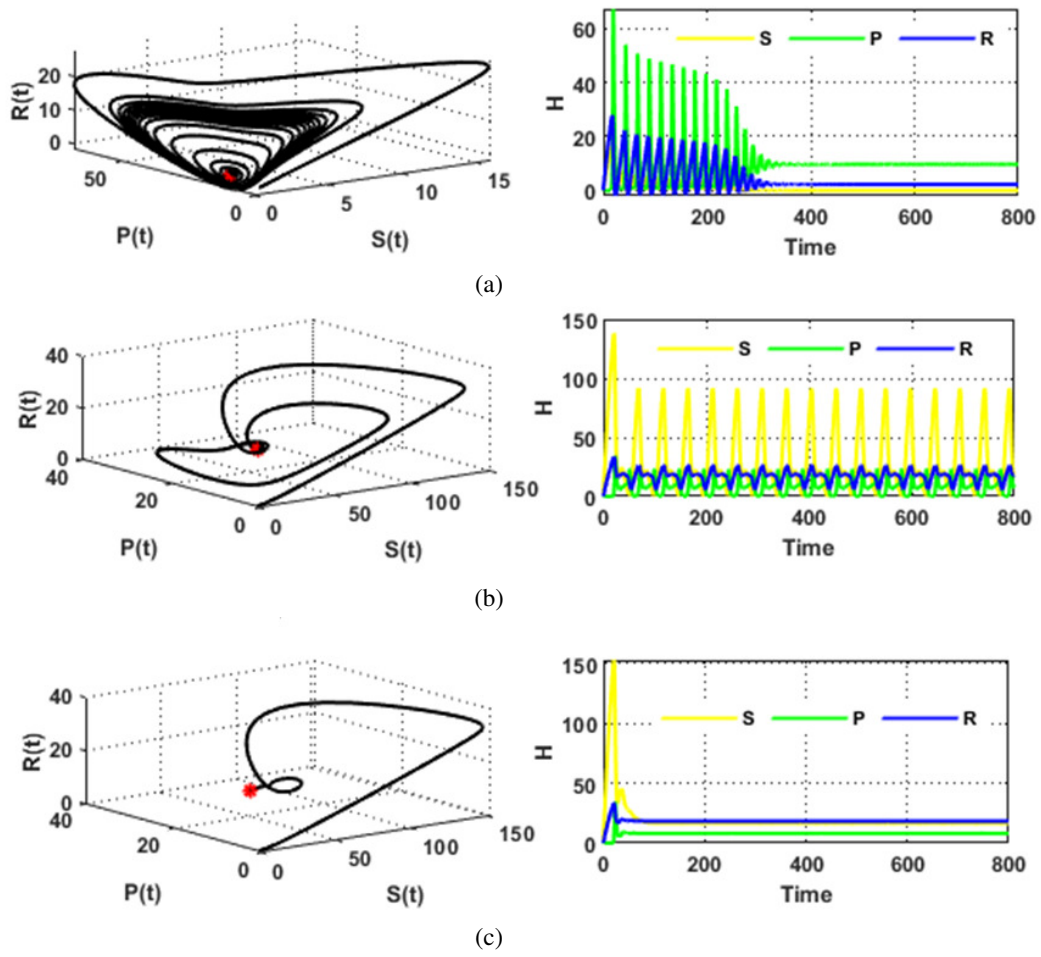

Figure 12. Phase portrait and time series of the SPR model with an increased value of A: a) Emergence of a Hopf bifurcation is reached when $A = 1.24$; b) Occurrence of two-period oscillation when the parameter $A = 9$; c) The coexistence point of the SPR is attained when $A = 9.6$.

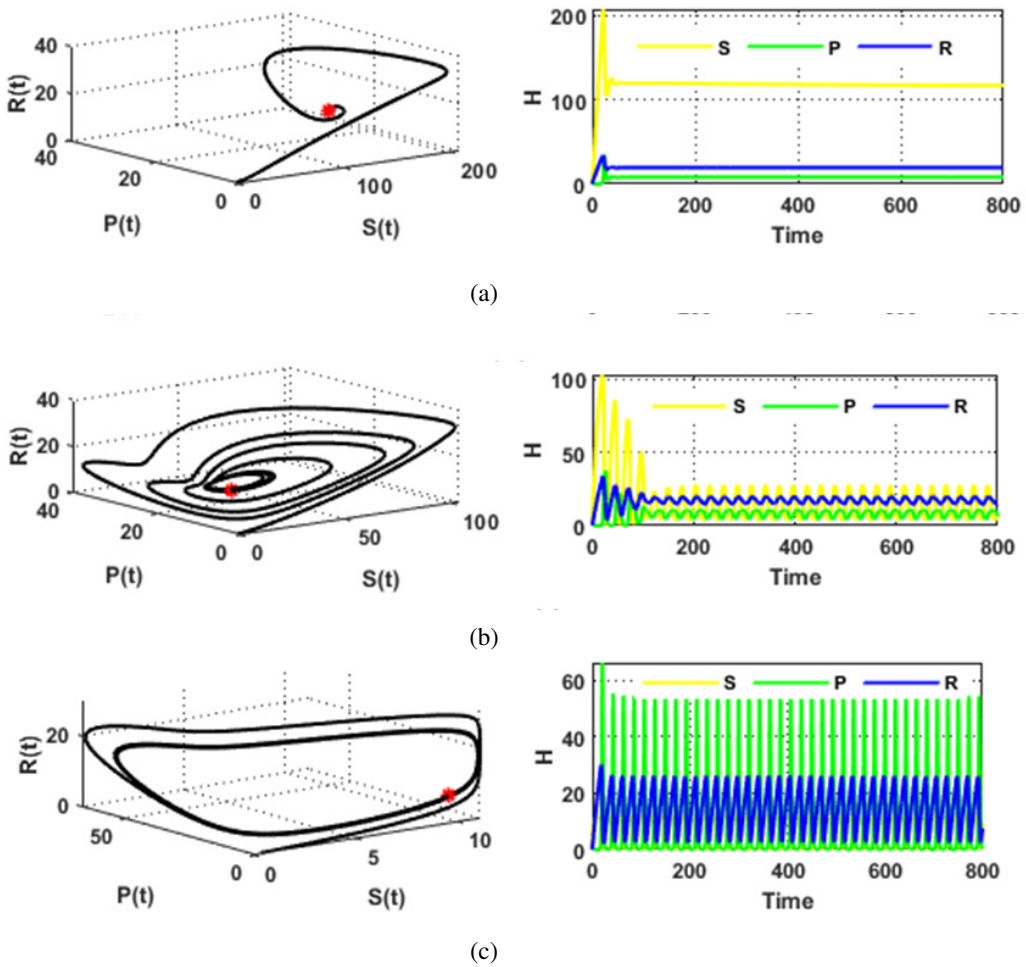

Figure 13. Phase portrait and time series of the SPR model with an increased value of μ_0: a) The coexistence point of the SPR is attained when $\mu_0 = 0.0003$; b) Emergence of a Hopf bifurcation is reached when $\mu_0 = 0.075$; c) Occurrence of a two-period oscillation when the parameter $\mu_0 = 0.24$.

Figure 14 demonstrates that an important dynamic: in the absence of revegetation initiatives (e), P and R go to extinction, and the system is stable at the desertification point H_1 (Figure 14a). At lower values of e, when $e \in (0, 0.02)$, only P goes to extinction from the system (Figure 14b). For higher values of e, when $e \in [0.02c, 0.45)$, the system stabilized at the interior equilibrium H_4 (Figure 14c). This result shows a transcritical bifurcation occurring at $e^{TB} = 0.02$. Eventually, the system becomes periodic for $e \geq 0.45$ (Figure 14c). That means the Hopf bifurcation occurs at $e^{HB} = 0.45$. Figure 15 shows that r can stabilize the system.

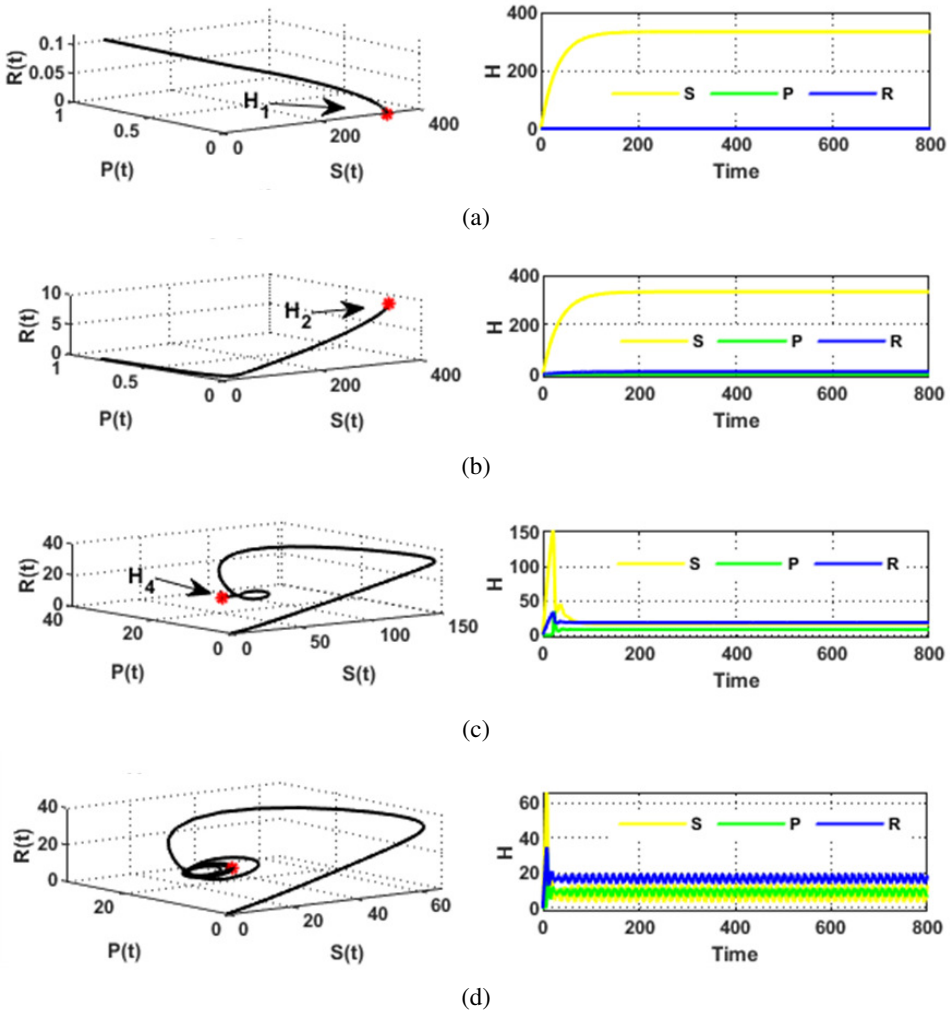

Figure 14. Phase portrait and time series of the SPR model with an increased value of e: a) The desertification point within the SPR system is possible for $e = 0$; b) The plant-free point is achievable at $e = 0.02$; c) The coexistence point of the SPR is attained when $e = 0.2$; d) Oscillations within the SPR system occur at $e = 0.45$.

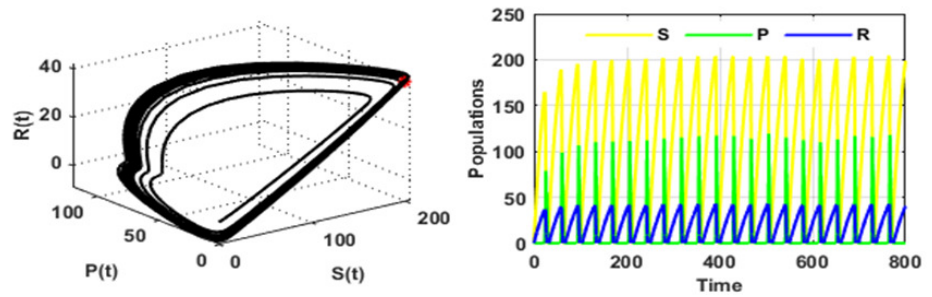

(a)

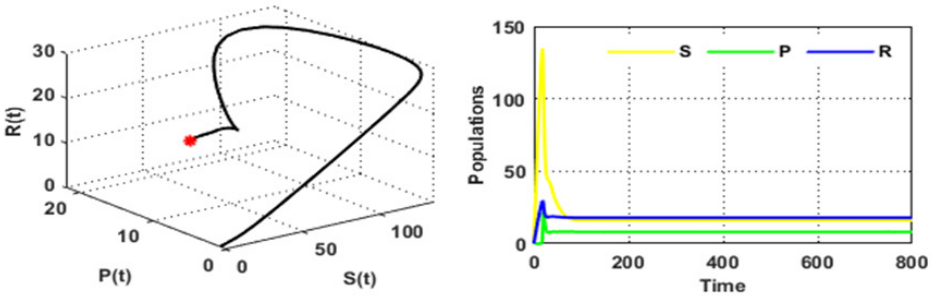

(b)

Figure 15. The impact of the parameter r within the SPR system: a) Oscillations within the SPR system occur at $r = 0.21$; b) Coexistence within the SPR system is achievable at $r = 0.22$.

A global sensitivity analysis using Partial Rank Correlation Coefficients (PRCCs) was conducted to identify the parameters most strongly influencing the long-term dynamics of airborne dust pollutants and plant biomass. Figure 16 indicates that increasing the parameters $A, \mu_1, \mu_2 b$, and ω lead to a significant rise in airborne dust concentration, whereas the parameters $\mu_0 \alpha, r, k$ and γ lead to a significant reduction in airborne dust concentration. Figure 17 demonstrates that increases in the parameters r, α, μ_0, k, e and γ positively contribute to plant biomass growth and promote persistence/oscillation/chaos. Furthermore, the parameters A, μ_1, μ_2 and β eexhibit the strongest negative effects on plant biomass growth rate.

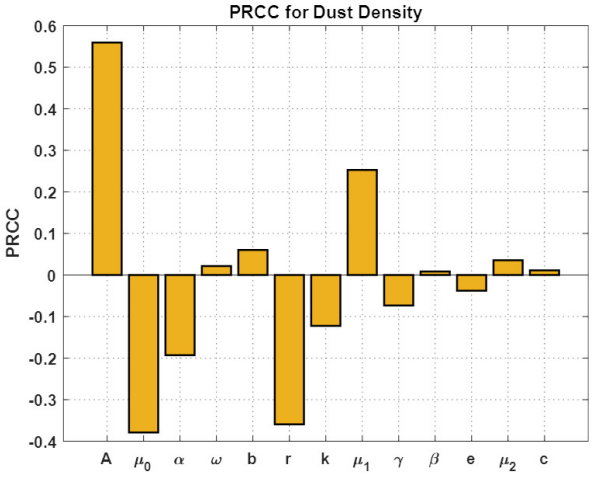

Figure 16. PRCC analysis of the dust pollutant dynamics in the SPR system.

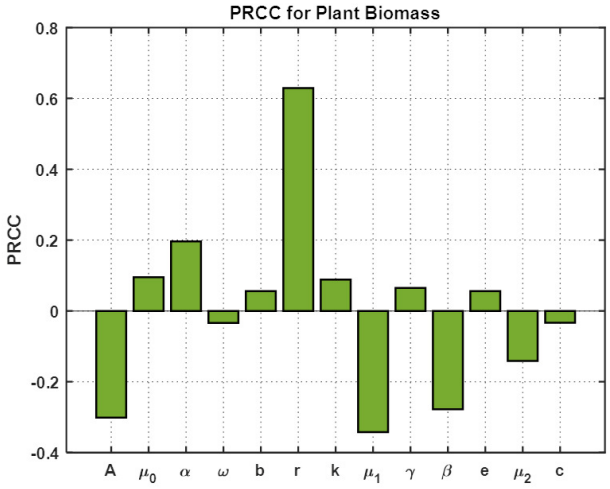

Figure 17. PRCC analysis of the plant biomass dynamics in the SPR system.

9. Conclusion

Here, we examine the Dust-Plant-Revegetation (SPR) model while incorporating the Allee effect in plants and the influence of the wind effect. First, the positivity and boundedness of the proposed system have been established. Then, the feasible equilibrium points have been determined and analyzed for their local and global stability. Furthermore, the occurrence of saddle, transcritical, and Hopf bifurcations has been theoretically proven. From the numerical simulations, critical transitions in system stability, particularly the emergence of periodic and chaotic dynamics influenced by variations in wind intensity, dust depletion efficiency, and plant growth rates, have been observed. The identification of generalized Hopf (GH) bifurcation points highlights the significance of nonlinear feedback mechanisms in shaping system behavior. These findings suggest that even small perturbations in environmental parameters can lead to drastic shifts in ecosystem stability. Furthermore, we observe that as the value of bb increases, the system transitions from chaotic dynamics to stability, indicating that chaos can be controlled. These results underscore the importance of revegetation initiatives in mitigating dust storms and stabilizing plant biomass levels. The transition from stability to chaos indicates that uncontrolled environmental disturbances, such as extreme wind conditions or reduced revegetation activities, may lead to persistent instability and ecosystem degradation. This study contributes to the understanding of ecosystem resilience and provides a mathematical framework for designing effective environmental policies aimed at maintaining long-term ecological balance. It could be concluded that raising the implementation rate for revegetation initiatives within appropriate ranges can stabilize the system at a positive stable point or a stable periodic case. These additions provide more quantitative guidance for sustainable environmental management strategies designed to improve vegetation management and reduce the concentration of dispersed pollution.

Future research could explore optimal control strategies and the impact of stochastic environmental variations on system stability.

Author contributions statement

All authors have contributed equally to this work.

Compliance with ethical standards

Conflicts of interest regarding the publishing of this work, the authors certify that they have no conflicts of interest.

Data availability statements

All of the data generated or analyzed during this investigation are included in this paper.

REFERENCES

1. B. Fan, L. Guo, N. Li, J. Chen, H. Lin, X. Zhang, M. Shen, Y. Rao, C. Wang, and L. Ma, *Earlier vegetation green-up has reduced spring dust storms*, Scientific Reports, vol. 4, no. 1, p. 6749, 2014.
2. E. Hakeem, S. Jawad, A. H. Ali, M. Kallel, and H. A. Neamah, *How mathematical models might predict desertification from global warming and dust pollutants*, MethodsX, vol. 14, p. 103259, 2025.
3. X. Long, X. Tie, G. Li, J. Cao, T. Feng, S. Zhao, L. Xing, and Z. An, *Effect of ecological restoration programs on dust concentrations in the North China Plain: a case study*, Atmospheric Chemistry and Physics, vol. 18, no. 9, pp. 6353–6366, 2018.
4. M. Abdelkader, S. Metzger, R. E. Mamouri, M. Astitha, L. Barrie, Z. Levin, and J. Lelieveld, *Dust–air pollution dynamics over the eastern Mediterranean*, Atmospheric Chemistry and Physics, vol. 15, no. 16, pp. 9173–9189, 2015.
5. A. M. Farmer, *The effects of dust on vegetation—a review*, Environmental Pollution, vol. 79, no. 1, pp. 63–75, 1993.
6. A. A. Thirthar, A. L. Alaoui, S. Roy, and P. K. Tiwari, *Fractional and stochastic dynamics of predator–prey systems: The role of fear and global warming*, European Physical Journal B, vol. 98, no. 7, pp. 1–21, 2025.
7. S. Sundar, and R. Naresh, *Modeling the effect of dust pollutants on plant biomass and their abatement from the near earth atmosphere*, Modeling Earth Systems and Environment, vol. 3, no. 1, p. 42, 2017.
8. M. Ahmed and S. Jawad, *The role of antibiotics and probiotics supplements on the stability of gut flora bacteria interactions*, Communications in Mathematical Biology and Neuroscience, vol. 2023, pp. 1–20.
9. Z. Aamer, S. Jawad, B. Batiha, A. H. Ali, F. Ghanim, and A. A. Lupaş, *Evaluation of the dynamics of psychological panic factor, glucose risk and estrogen effects on breast cancer model*, Computation, vol. 12, no. 8, p. 160, 2024.
10. A. K. Misra, M. Verma, and E. Venturino, *Modeling the control of atmospheric carbon dioxide through reforestation: effect of time delay*, Modeling Earth Systems and Environment, vol. 1, no. 3, p. 24, 2015.
11. F. Nezar, S. Jawad, M. Winter, and A. Zeb, *Stability analysis of excessive carbon dioxide gas emission model through following reforestation policy in low-density forest biomass*, Baghdad Science Journal, vol. 22, no. 4, pp. 1335–1353, 2025.
12. A. A. Thirthar, B. A. Sharba, S. J. Majeed, P. Panja, and T. Abdeljawad, *The dynamics of prey–predator model with global warming on carrying capacity and wind flow on predation*, Nonlinear Engineering, vol. 15, no. 1, p. 20250182, 2026.
13. S. Jawad, A. A. Thirthar, and K. S. Nisar, *The impact of climate change on flowering plants-bees-Vespa orientalis model*, Results in Control and Optimization, vol. 20, p. 100583, 2025.
14. S. Jawad, A. A. Thirthar, P. Panja, and T. Abdeljawad, *Effects of wind, global warming and fear in a disease-induced Hassell-Varley predator-prey model through Caputo fractional order derivative*, International Journal of Modelling and Simulation, pp. 1–19, 2026.
15. N. J. Balfour and F. L. Ratnieks, *Wind alters plant-pollinator community structure, bee foraging rate and movements between plants*, Behavioral Ecology, vol. 36, no. 4, p. araf067, 2025.
16. B. Dubey, S. Sharma, P. Sinha, and J. B. Shukla, *Modelling the depletion of forestry resources by population and population pressure augmented industrialization*, Applied Mathematical Modelling, vol. 33, no. 7, pp. 3002–3014, 2009.
17. S. Jawad, S. Roy, A. A. Thirthar, and P. K. Tiwari, *Deterministic and stochastic risks assessment of excessive CO2 emission on forest biomass under weak Allee effect*, Journal of Applied Mathematics and Computing, vol. 71, no. 6, pp. 9129–9156, 2025.
18. S. M. Pawson, A. Brin, E. G. Brockerhoff, D. Lamb, T. W. Payn, A. Paquette, and J. A. Parrotta, *Plantation forests, climate change and biodiversity*, Biodiversity and Conservation, vol. 22, no. 5, pp. 1203–1227, 2013.
19. J. M. Hartwick, *Deforestation and population increase*, In: Institutions, sustainability, and natural resources: institutions for sustainable forest management, Chapter 8, Springer, Berlin, pp. 155–191, 2005.
20. D. Barman, J. Roy, and S. Alam, *Impact of wind in the dynamics of prey–predator interactions*, Mathematics and Computers in Simulation, vol. 191, pp. 49–81, 2022.
21. M. Ahmed, S. Jawad, D. Das, S. Boulaaras, and M. S. Osman, *Impact of dust storms on plant biomass: Model structure and dynamic study*, Alexandria Engineering Journal, vol. 126, pp. 605–622, 2025.
22. P. Hartman, *Ordinary Differential Equations*, 2nd ed., SIAM, Philadelphia, PA, 2002.
23. L. Perko, *Differential equations and dynamical systems*, vol. 7, Springer Science & Business Media, 2013.
24. J. P. LaSalle, *Stability theory and invariance principles*, In: L. Cesari, J. K. Hale, and J. P. LaSalle (eds.), Dynamical Systems, pp. 211–222, Elsevier, New York, 1976.
25. M. Ahmed and S. Jawad, *Bifurcation analysis of the role of good and bad bacteria in the decomposing toxins in the intestine with the impact of antibiotic and probiotics supplement*, AIP Conference Proceedings, vol. 3097, no. 1, p. 080033, 2024.
26. S. K. Hassan and S. R. Jawad, *The effect of mutual interaction and harvesting on food chain model*, Iraqi Journal of Science, vol. 63, no. 6, pp. 2641–2649, 2022.
27. D. Mukherjee, *Study of fear mechanism in predator-prey system in the presence of competitor for the prey*, Ecological Genetics and Genomics, vol. 15, p. 100052, 2020.